ACS Catalysis

Review

pubs.acs.org/acscatalysis

Iridium As Catalyst and Cocatalyst for Oxygen Evolution/Reduction in Acidic Polymer Electrolyte Membrane Electrolyzers and Fuel Cells

Ermete Antolini

Scuola di Scienza dei Materiali, Via 25 aprile 22, 16016 Cogoleto, Genova, Italy

ABSTRACT: Among noble metal electrocatalysts, only iridium presents high activity for both the oxygen reduction reaction (ORR) in acid medium, in the oxide form, and the oxygen evolution reaction (OER) in acid medium, alloyed with first row transition metals. Indeed, platinum, the best catalyst for the ORR, has poor activity for the OER in any form, and ruthenium, the best catalyst for the OER, in the oxide form, possess poor activity for the ORR in any form. In this work, an overview of the application of Ir and Ir-containing catalysts for the OER in proton-exchange membrane water electrolyzer anodes, for the ORR in proton exchange membrane fuel cell cathodes, and for both OER and ORR in unit regenerative fuel cell oxygen electrodes is presented.

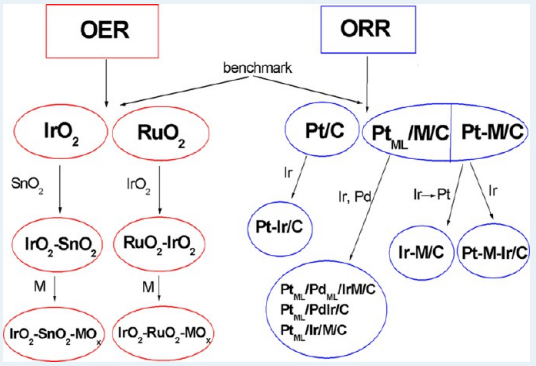

KEYWORDS: *iridium, oxygen reduction, oxygen evolution, water electrolyzers, fuel cells*

1. INTRODUCTION

1.1. Proton Exchange Membrane Fuel Cells (PEMFCs) and Water Electrolyzer (PEMWEs). Proton exchange membrane (PEM) is used both in low-temperature fuel cells (PEMFCs)[1] and water electrolyzer (PEMWEs).[2] The PEM (commonly Nafion) provides high proton conductivity and low gas crossover. The configurations of a PEMFC and a PEMWE are similar, formed by a membrane electrode assembly (MEA), current collectors, and bipolar plates with flow channels. The MEA consists of two electrodes (anode and cathode), which are each coated on one side with a thin catalyst layer and separated by a PEM. The main difference between PEMFCs and PEMWEs is related to the oxygen catalyst: In PEMFCs, carbon-supported Pt and Pt alloys are used as the cathode catalyst for the oxygen reduction reaction (ORR). In PEMWEs, noble metal oxides, such as IrO_2 and RuO_2—but not PtO_2—are utilized as the anode catalyst for the anodic oxygen evolution reaction (OER).

1.2. Oxygen Reduction in Acid Medium. The ORR is a multielectron reaction, consisting of a number of elementary steps and different reaction intermediates.[3] O_2 electroreduction in acid media can occur through different pathways; among them, the main pathways are a "direct" four-electron reduction to H_2O and a two-electron pathway involving reduction to H_2O_2. For Pt, O_2 electroreduction commonly takes place by the four-electron reduction pathway. For less active metals, such as Au and Hg, O_2 electroreduction takes place instead by the two-electron reduction pathway. For the first electron transfer step, Damjanovic and Brusic[4] suggested that both the proton and the charge transfer take place at the same time, and the proton transfer is the rate-determining step (rds). According to Damjanovic's theory, both a mechanism with oxygen electrochemisorption,

$$O_2 + Pt + H^+ + e^- \rightleftharpoons Pt\text{-}O_2H_{ads} \quad (1)$$

$$Pt\text{-}O_2H_{ads} + 3H^+ + 3e^- \rightleftharpoons Pt + 2H_2O \quad (2)$$

and an electrochemical−chemical−electrochemical (ECE) mechanism with the following steps and adsorbed intermediate species OH_{ads} and O_2H_{ads},

$$O_2 + Pt + H^+ + e^- \rightleftharpoons Pt\text{-}O_2H_{ads} \quad (1)$$

$$Pt\text{-}O_2H_{ads} + H_2O \rightleftharpoons 3Pt\text{-}OH_{ads} \quad (3)$$

$$3Pt\text{-}OH_{ads} + 3H^+ + 3e^- \rightleftharpoons 3H_2O \quad (4)$$

were proposed. The reaction is first-order with respect to O_2 pressure in the whole range of potentials. At a high potential and high amount of adsorbed oxygenated species, the Tafel slope is 60 mV dec^{-1}. At a low potential and low amount of adsorbed oxygenated species, the Tafel slope is 120 mV dec^{-1}.

1.3. Oxygen Evolution in Acid Medium. On the other hand, the following mechanism was proposed for the OER in acid medium on active oxide electrodes.[5] For the first step, a charge-transfer step going through the formation of an adsorbed hydroxy species onto a surface active site M is proposed.

$$M + H_2O \rightarrow M - OH_{ads} + H^+ + e^- \quad (5)$$

The second step can occur through either an electrochemical oxide path with a second electron transfer,

$$M - OH \rightarrow M - O_{ads} + H^+ + e^- \quad (6)$$

Received: September 18, 2013
Revised: February 23, 2014
Published: March 19, 2014

   dx.doi.org/10.1021/cs4011875 | ACS Catal. 2014, 4, 1426−1440

or an oxide path with a recombination step.

$$M - OH + M - OH \rightarrow M - O + M + H_2O \quad (7)$$

Then the formation of O_2 and two active sites occurs (third step).

$$2M - O_{ads} \rightarrow 2M + O_{2(g)} \quad (8)$$

The following Tafel slopes result from this mechanism: 120 mV dec^{-1} for step 5, 40 mV $decade^{-1}$ for step 6, 30 mV dec^{-1} for step 7, and 15 mV dec^{-1} for step 8. To obtain a Tafel slope of 60 mV dec^{-1}, such as on IrO_2-based catalysts at low current range, step 5 can be substituted by the following subreactions,

$$M + H_2O \rightarrow M - OH^*_{ads} + H^+ + e^- \quad (9)$$

$$M - OH^*_{ads} \rightarrow M - OH_{ads} \quad (10)$$

in which adsorption intermediates $M-OH^*_{ads}$ and $M-OH_{ads}$ possess the same chemical structure but different energy states. Steps 6 and 7 are alternative or can occur in parallel. The different pathways and Tafel slopes for various oxide catalysts depend on the strength of adsorption of the intermediate and the composition of the oxide layer, respectively.[6]

Among noble metal electrocatalysts, only iridium presents high activity for both the oxygen reduction reaction, in the oxide form, and the oxygen evolution reaction, alloyed with first row transition metals. Indeed, platinum, the best catalyst for the ORR, has poor activity for the OER in any form, and ruthenium, the best catalyst for the OER, in the oxide form possesses poor activity for the ORR in any form. In this work, an overview of the application of Ir and Ir-containing catalysts for the OER in PEMWE anodes, for the ORR in PEMFC cathodes (both in acid medium), and for both OER and ORR in unit regenerative fuel cell (URFC) oxygen electrodes, is presented.

2. BINARY/TERNARY IRO_2-CONTAINING CATALYSTS AND NANOSTRUCTURED IRO_2 CATALYSTS FOR THE OXYGEN EVOLUTION IN PEMWES

2.1. IrO_2-Based Mixed Oxides. IrO_2 and RuO_2 are promising oxygen anode catalysts.[7] IrO_2 has been preferentially used as an anode electrocatalyst because of its higher stability corrosion resistance in PEMWE conditions than that of RuO_2, although its electrochemical activity is slightly lower than that of RuO_2.[7−9] However, the use of pure IrO_2 is limited by high costs and a short electrode lifetime, so mixed oxides formed by dispersing the noble metal oxide in a more stable nonprecious matrix are intensively investigated. Mixed oxides consisting of low-cost oxides, such as SnO_2, Ta_2O_5, Nb_2O_5, TiO_2 and SiO_2, and IrO_2, allow the reduction of the amount of the noble metal in the electrode without a significant decrease in the catalytic activity and electronic conductivity. Moreover, the addition of nonprecious metal oxides to IrO_2 improves its stability against corrosion. As for PEMFC catalysts,[10] the nonprecious metal oxides serve mainly as a substrate for the active catalyst, but they can have an effect on the specific activity of IrO_2. On the other hand, the addition of RuO_2 to IrO_2 should enhance its OER activity. Among mixed oxides, IrO_2-RuO_2 and IrO_2-SnO_2 are the most interesting.

2.1.1. Addition of RuO_2 As an Active Oxide to IrO_2. *2.1.1.1. Binary IrO_2-RuO_2 Catalysts.* Mixing RuO_2 and IrO_2 should retain the helpful properties (high activity of RuO_2 and high stability of IrO_2) of both components.[11] Ir in IrO_2-RuO_2 can act either as catalyst in Ir-rich mixed oxides (where the presence of Ru increases the activity of Ir) or as a cocatalyst in Ru-rich mixed oxides (in which the presence of Ir increases the stability of Ru). Mixed Ir−Ru oxides can be prepared in different ways: films may be obtained by reactive sputtering[11] and spray deposition;[12] fine powders, by hydrolysis,[13] thermal decomposition[14,15] and the Adams fusion method.[16,17] For oxides synthesized by chemical methods, the formation of an atomic mixture is supported by aqueous solvents; on the other hand, organic solvents give rise to Ir segregation on the catalyst surface.[18] The mixed oxide may be present either as a homogeneous $Ir_xRu_{1-x}O_2$solid solution,[12,13,16] or as IrO_2 and RuO_2 separate phases.[19]

Ir segregation on the catalyst surface was observed on thermally[14,18] and hydrothermally[13] prepared binary Ir−Ru oxides. Reactively sputtered IrO_2-RuO_2 catalysts, on the other hand, did not present surface segregation.[11] Likely the surface enrichment of one of the components increases with decreasing the mixture homogeneity.[18] Along with the increase in ruthenium content in the $Ir_xRu_{1-x}O_2$, the average particle size of catalysts increased.[15] Obviously, atomic mixing, surface segregation, and particle size depend on the synthesis method. Generally, the $Ir_xRu_{1-x}O_2$ compounds are more active than IrO_2 and more stable than RuO_2.[11−22]

A remarkable increase in the stability of IrO_2-RuO_2 compared with RuO_2 was observed.[11,16] Kotz and Stucki[11] observed that a small amount of IrO_2 (20%) in RuO_2 results in a considerable decrease in the corrosion rate of RuO_2. By chronopotentiometry measurements at 50 mA cm^{-2}, Cheng et al.[16] found that on RuO_2, the potential considerably increases after about 20 000 s. Conversely, $Ir_{0.2}Ru_{0.8}O_2$ was much more stable than RuO_2, and the potential was nearly constant up to 40 000 s. The dependence of Tafel slope and OER activity, expressed as the IrO_2-RuO_2-to-RuO_2 OER potential ratio, on the Ru content for various data sets, at a constant current density for each data set in the range 0.1−10 mA cm^{-2}, are shown in Figures 1 and 2, respectively. As

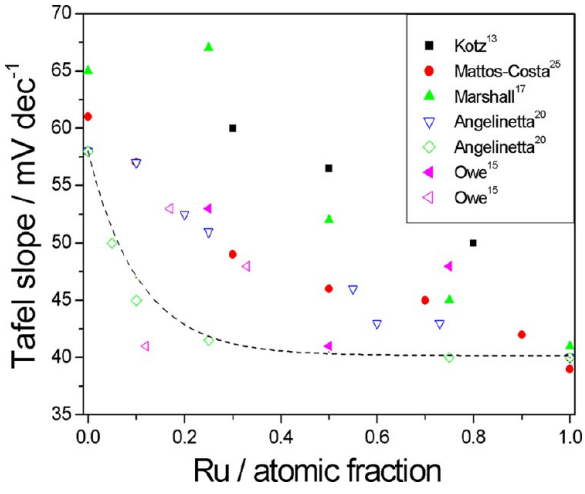

Figure 1. Tafel slope of IrO_2-RuO_2 as a function of Ru content for various data sets. Solid symbols, bulk Ru content; open symbols, surface Ru content. Dashed line calculated assuming a linear combination of IrO_2 and RuO_2 properties from ref 11.

can be seen in Figures 1 and 2, the experimental values of the binary oxide considerably differ from the values obtained by the sum of the values of the single oxides, as reported in ref 11 (dashed lines). The difference between experimental and theoretical values could depend on Ir segregation on the catalyst surface. The data of Owe et al.[13] for the OER activity and those of Angelinetta et al.[18] (for IrO_2-RuO_2 obtained by precursors in

dx.doi.org/10.1021/cs4011875 | ACS Catal. 2014, 4, 1426−1440

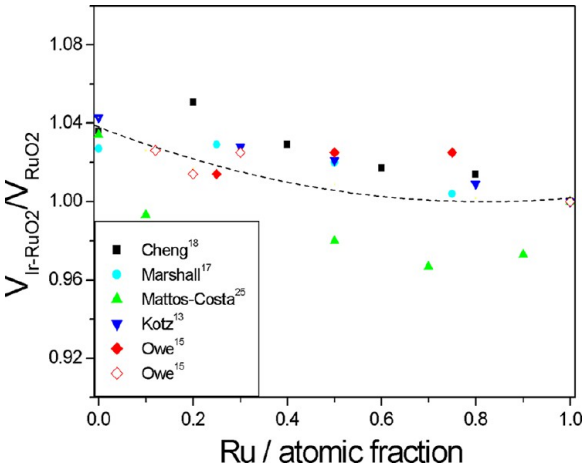

Figure 2. Dependence of the OER activity, expressed as the IrO_2–RuO_2-to-RuO_2 OER potential ratio, on Ru content for various data sets at a constant current density for each data set in the range 0.1–10 mA cm^{-2}. Solid symbols, bulk Ru content; open symbols, surface Ru content. Dashed line calculated assuming a linear combination of IrO_2 and RuO_2 properties from ref 11

nonaqueous solution) for Tafel slope, expressed in terms of surface composition, seem to support this hypothesis. Indeed, these data are in agreement with those obtained by a linear combination of IrO_2 and RuO_2 properties, but the data of Owe et al.[13] and Angelinetta et al.[18] (for IrO_2–RuO_2 obtained by precursors in aqueous solution) for the Tafel plot, also expressed in terms of surface composition, do not match with calculated values. Thus, Ir surface segregation does not fully explain the electrochemical results.

To explain the large effect of small IrO_2 contents on RuO_2 activity, the O_2 evolution mechanisms were analyzed. Both Ru corrosion and O_2 evolution go on through the formation of RuO_4,[11] so during the O_2 evolution process, the t_{2g} band contains at most 2 electrons. For Ir, oxygen is released from IrO_3, so during O_2 evolution, 3–5 electrons populate the t_{2g} band.[11] Considering the formation of a common band for the mixed oxides, shows that Ir–Ru alloying precludes the oxidation of RuO_2 to RuO_4. The suppression of RuO_4 formation results in less corrosion but also lower O_2 evolution activity of Ru sites.

2.1.1.2. Ternary IrO_2–RuO_2-Based Catalysts. To increase the active surface area, in particular for catalysts prepared by the Adams fusion method, and the stability of $Ir_xRu_{1-x}O_2$, inert nonprecious oxides were added to the noble metal mixed oxides.[23−27] Ir segregation on the catalyst surface was observed also on ternary Ir–Ru–M (M = Ti, Sn) oxides.[23,24] First, Hutchings et al.[24] prepared a ternary $Ir_{0.25}Ru_{0.25}Sn_{0.5}O_2$ catalyst by the Adams method and compared its OER activity and stability with that of IrO_2 and $Ir_{0-5}Ru_{0.5}O_2$. The ternary catalyst showed an initially lower OER activity, but a much improved stability, resulting in a higher activity than that of IrO_2 and IrO_2–RuO_2 after 320 and 780 h of live testing, respectively.

Marshall et al.[25] synthesized $Ir_xRu_yTa_zO_2$ powders by a hydrothermal method. Catalysts containing 20–40 mol % Ru and 0–20 mol % Ta presented high performance in PEMWEs. In most cases up to 20 mol %, the addition of Ta to Ir–Ru oxides does not appreciably decrease the cell performance. This could increase the durability of these catalysts. Conversely, in addition to an increase in the stability, the addition of Mo or Co oxide also increases the OER activity of IrO_2–RuO_2.[26,27] $Ir_{0.4}Ru_{0.6}Mo_xO_y$ prepared by a modified Adams' fusion method presented a much smaller particle size and larger electrochemically active surface area (ECSA) compared with $Ir_{0.4}Ru_{0.6}O_2$.[26] Single cell performance proved that $Ir_{0.4}Ru_{0.6}Mo_xO_y$ has a higher OER activity than $Ir_{0.4}Ru_{0.6}O_2$. The increase in the ECSA was the primary reason for the increase in the performance. Ru–Ir–Co oxides prepared by chemical reduction showed slightly better catalytic activity than Ru–Ir oxides.[27] Tafel slopes of Ru–Ir oxides in both low and large overpotentials were higher than those of Ru–Ir–Co oxides.

2.1.2. Addition of SnO_2 As an Inert Oxide to IrO_2.
2.1.2.1. Binary IrO_2–SnO_2 Catalysts. Although carbon is commonly used as an electrocatalyst support in PEMFCs,[28] its use in PEMWEs is not appropriate. Carbon has a low equilibrium potential for carbon corrosion and is thermodynamically unstable above the equilibrium potential, as shown in the following reactions.[29]

$$C + 2H_2O \rightarrow CO_2 + 4H^+ + 4e^- \quad E^0 = 0.207 \text{ V vs SHE} \tag{11}$$

$$C + H_2O \rightarrow CO + 2H^+ + 2e^- \quad E^0 = 0.518 \text{ V vs SHE} \tag{12}$$

Because PEMWE anodes operate at high anodic potentials (>1.5 V vs SHE), the utilization of carbon in the PEMWE anode structure has to be avoided. Among various inert-metal oxides, SnO_2, because of its elevated conductivity and stability at high temperature,[12] which makes it a suitable PEMWE electrocatalyst support, was the most interesting and was extensively investigated in binary IrO_2–SnO_2 catalysts with respect to oxygen evolution in an acid medium.[17,22,30−33] Mixed Ir–Sn oxides were prepared mainly by the Adams' fusion method.[17,22,32,34,35] Other synthesis methods, such as thermal decomposition,[30,36] a sol–gel method,[37] a modified polyol method,[31] and a surfactant-assistant method,[33] were also used. The crystal structure and lattice parameters of IrO_2 and SnO_2 are similar. The ionic radius of Ir^{4+} (0.077 nm) is similar to that of Sn^{4+} (0.083 nm). These similar physical characteristics of IrO_2 and SnO_2 allow the formation a tetragonal $Sn_xIr_{1-x}O_2$ solid solution. Generally, $Sn_xIr_{1-x}O_2$ solid solutions were obtained by different preparation methods.[19,26,31,33,36,37] In various cases, however, two separate phases were obtained, formed by two saturated solid solutions: a SnO_2-rich phase and an IrO_2-rich phase.[32−36] Xu et al.[32] ascribed the formation of two separate phases to the use of SnO_2 as the precursor (it is thought that nonconductive or semiconducting SnO_2 crystals may be covered by IrO_2). IrO_2 segregation on IrO_2–SnO_2 catalyst surface takes place; as a consequence, at nominal 20 mol % IrO_2, the amount of IrO_2 on the surface attains more than 80 mol %.[33,34,38] IrO_2–RuO_2–SnO_2 ternary catalysts also exhibited noble metal segregation.[23] On the other hand, Balko and Nguyen[39] reported SnO_2 segregation on IrO_2–SnO_2 catalyst surface. According to Marshall et al.,[35] in IrO_2–SnO_2 binary catalysts, a slight SnO_2 surface segregation (5–10 mol %) was observed.

Conflicting results regarding the effect of Sn addition on the OER activity of Ir have been reported. De Pauli and Trasatti[30] found that, consistently with the remarkable IrO_2 segregation on the catalyst surface, the OER activity of Ir–Sn oxides increases considerably up to ~20 mol % IrO_2 and remains almost constant at higher IrO_2 contents. As shown in Figure 3, the Tafel slope was nearly constant in the 55–60 mV dec^{-1} range for compositions of 10–100 mol % IrO_2. For IrO_2 contents ≤10 mol %, the Tafel slope increased with increasing SnO_2 content to approach 120 mV dec^{-1} for pure SnO_2. The current density normalized to unit

dx.doi.org/10.1021/cs4011875 | ACS Catal. 2014, 4, 1426–1440

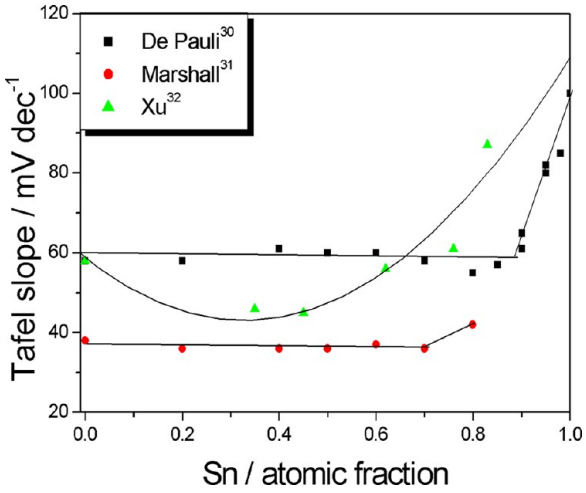

Figure 3. Tafel slope of IrO_2−SnO_2 as a function of Sn content for various data sets.

surface charge allows estimation o the specific OER activity. On this basis, considering the current density at 1.49 V vs RHE normalized to unit surface charge, a considerable increase in the OER specific activity with IrO_2 content up to ∼30−40% was observed, whereas geometric effects are effective at higher IrO_2 compositions. This behavior was tentatively explained considering that the range of lower IrO_2 contents is characterized by transition from metallic to semiconducting properties.[30] It can be supposed that the electronic structure of IrO_2 is affected by that of SnO_2.

As can be seen in Figure 4, dividing the current density per geometric area by the Ir content in the catalyst, the resulting Ir-

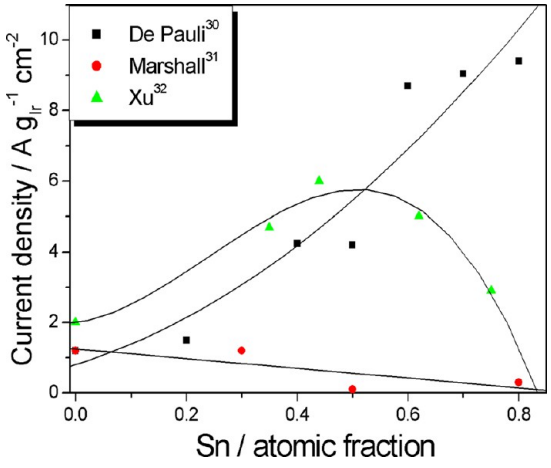

Figure 4. Dependence of Ir-normalized current density on Sn content for various data sets. (black box, red circle) E = 1.49 V vs RHE; (green triangle) E = 1.22 V vs SCE, current density/10.

normalized OER activity increases with increasing Sn content up to 80% Sn, essentially due to Ir enrichment on the catalyst surface. Conversely, Marshall et al.,[31] by potential measurements at 1 mA cm^{-2} observed that the OER activity of Ir−Sn oxides decreases with increasing Sn content. Because in this case, Ir segregation does not occur, the main effect of SnO_2 is to dilute IrO_2. Because the potential of $Ir_{0.8}Sn_{0.2}O_2$ is similar to that of IrO_2, however, the same performance is attained with a lower IrO_2 amount. The Tafel slope was almost constant with values around 36 mV dec^{-1}, except for the highest Sn contents, which showed a Tafel slope of 42 mV dec^{-1}. As shown in Figure 3, apart from the absolute value, the dependence of the Tafel slope on the Sn content was similar to that observed by De Pauli and Trasatti.[30] The difference in the Tafel slope value has to be ascribed to the different rds for oxygen evolution on DSA electrodes[30] and these composite electrodes.

As for the results of De Pauli and Trasatti,[30] the current density normalized to unit surface charge allows estimation of the specific OER activity. The initial decrease in overall performance was only due to a decrease in the active area rather than a decrease in the specific activity. At ∼50−60 mol % Sn, the activity decreased and reached a new level at 70−80 mol % Sn. These results are similar to those on IrO_2−SnO_2 DSA electrodes (specific activity nearly constant at low Sn content).[30] As can be seen in Figure 4, unlikely from the results of De Pauli and Trasatti,[30] in the absence of Ir segregation on the surface, the Ir-normalized current density per geometric area does not increase, but slightly decreases with increasing Sn content owing to the increase in the crystallite size.

Finally, Xu et al.[32] found that the dependence of the potential at a current density in the range 10−50 mA cm^{-2} on Sn content in the catalyst goes through a minimum (at 33 wt % Sn). The dependence of the Tafel slope on tin content (Figure 3) presents the same trend as the potential, confirming the dependence of the catalytic activity on the Sn content. The maximum OER activity of IrO_2/SnO_2 (2:1) was ascribed to the mutual effects of an enhanced electrochemical surface area and the desorption of hydroxy species due to the lower electronegativity of tin than iridium.[40] As can be seen in Figure 4, the Ir-normalized current density per geometric area presents a maximum at ∼50 mol % Sn. The different activity of these Ir−Sn oxides[30−32] has to be ascribed to the different surface composition (presence or absence of Ir segregation) or to the different structure of the mixed oxide (solid solution or separate phases). By the analysis of voltammetric curves obtained at different scan rates, a high stability of IrO_2−SnO_2 catalysts was inferred.[38]

2.1.2.2. Ternary IrO_2−SnO_2-Based Catalysts. The OER activity of ternary Ir−Sn-based mixed oxides was also evaluated.[41−43] On the basis of the good performances of IrO_2−SnO_2, IrO_2−Ta_2O_5,[44,45] and IrO_2−Nb_2O_5[46] mixtures, ternary $Sn_{0.78}Ir_{0.15}Ta_{0.07}O_{2.175}$[41] and $Ir_{1-2x}Sn_xNb_xO_2$[42] nanostructures were investigated as OER electrocatalysts. Ardizzone et al.[41] prepared a $Sn_{0.78}Ir_{0.15}Ta_{0.07}O_{2.175}$ catalyst by a sol−gel route. $Sn_{0.78}Ir_{0.15}Ta_{0.07}O_{2.175}$ presented higher catalytic activity, expressed as current density normalized by weight of catalyst, than IrO_2 and binary SnO_2−IrO_2 catalysts. This is ascribed to the positive effect of Ta, which increases the surface area, improves the electronic conductance, and supports Ir surface segregation. Kadakia et al.[42] synthesized $Ir_{1-2x}Sn_xNb_xO_2$ solid solutions by thermal decomposition of a mixture of metal salt precursors on a Ti foil. Up to 40 mol % IrO_2, the OER activity, obtained by current density normalized by geometric area, of $Ir_{1-2x}Sn_xNb_xO_2$ was similar to that of pure IrO_2, whereas for 20 mol % IrO_2, the activity was only 20% lower. The $Sn_{0.5}Nb_{0.5}O_2$ support also improves the corrosion stability of IrO_2. Titanium anodes coated with a ternary iridium, antimony, and tin oxide mixture were investigated for the OER.[43] The Ti/IrO_x−Sb_2O_5−SnO_2 electrode containing only 10 mol % IrO_x showed a service life of 1600 h in a H_2SO_4 solution under a current density of 1 A cm^{-1} at 35 °C, as compared with 355 h for Ti/IrO_x.

On the basis of the high catalytic activity and stability of F-doped IrO_2,[47] Datta et al.[48] prepared a F-doped $(Sn_{0.80}Ir_{0.20})O_2$ catalyst. Notwithstanding its low IrO_2 content, this compound

dx.doi.org/10.1021/cs4011875 | ACS Catal. 2014, 4, 1426−1440

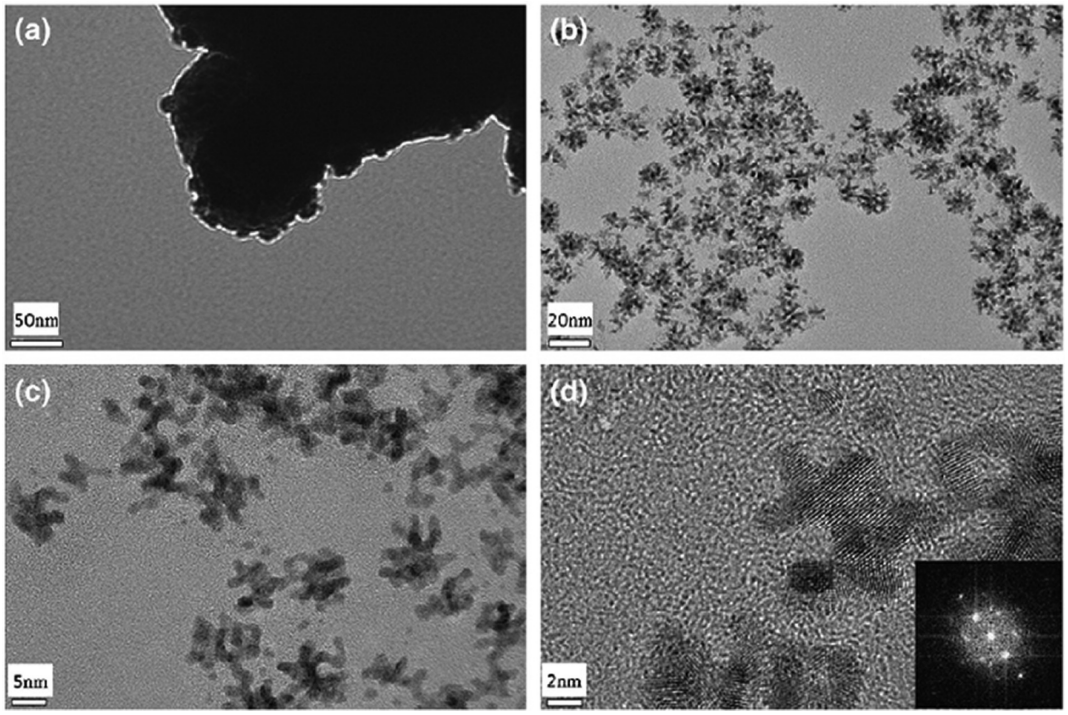

Figure 5. High-resolution transmission electron microscopy (HRTEM) images of (a) commercial Ir and (b–d) Ir dendritic nanoparticles at different magnifications. The inset image in part d shows the corresponding Fourier transform pattern of Ir nanodendrites. Reproduced from ref 49, copyright 2011, with permission from Elsevier.

displayed an OER activity and durability, obtained by current density normalized by geometric area, similar to that of pure IrO_2.

2.2. Nanostructured Ir and IrO_2 Catalysts. Another way to improve the efficiency of IrO_2 is the use of nanostructures with high surface area. It was found that the performance of catalysts for the OER strongly depends on their structural and morphological properties.[49−53] Ir nanodendrites (IrNDs)[49] were synthesized using tetradecyltrimethyl ammonium bromide (TTAB) as an organic capping agent.[49] After TTAB removal, the formation of an anodic IrO_2film on the surface of the IrNDs was observed. HRTEM images of IrNDs and a conventional Ir catalyst are shown in Figure 5. A higher OER activity of IrNDs than that of Ir nanoparticles was observed. Zhao et al.[50] reported a novel template-assisted deposition and etching strategy for fabricating IrO_2 nanotube arrays on conductive substrates. High-magnification SEM, TEM, and HRTEM images of as-prepared IrO_2 nanotube arrays are shown in Figure 6. The OER current at 1.2 V vs RHE, the turnover frequency (TOF), and the stability of IrO_2 nanotube arrays were higher than those of IrO_2 nanoparticles.

Mesoporous IrO_2 was prepared by soft[51] and hard[52] templating. In both cases, higher activity than nontemplated IrO_2 was observed.

Zhao et al.[53] synthesized an IrO_2–Au composite with a flower-like morphology. The nanoflowers displayed an OER activity and a TOF significantly higher than those for bare IrO_2 nanoparticles.

The OER activity and stability of binary and ternary IrO_2-based catalysts and nanostructured IrO_2 catalysts are summarized in Table 1.

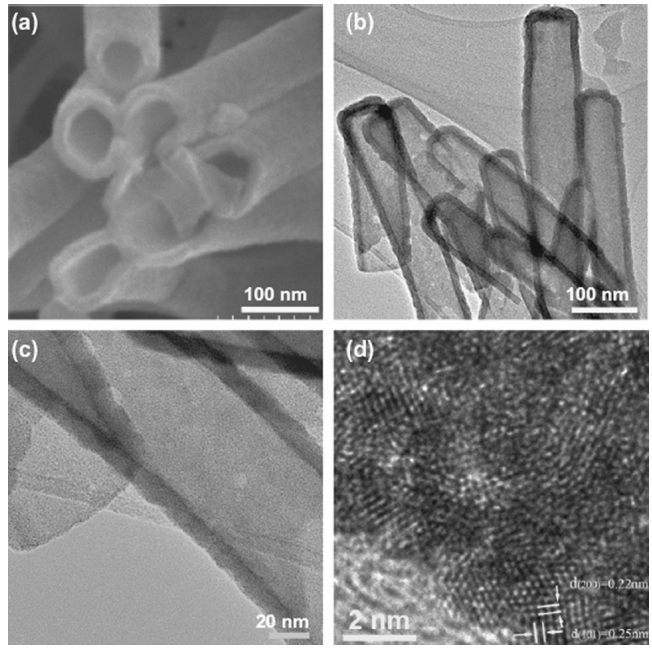

Figure 6. High-magnification scanning electron microscopy (SEM) (a), transmission electron microscopy (TEM) (b and c), and HRTEM (d) images of as-prepared IrO_2 nanotube arrays. Reproduced from ref 50, copyright 2013, with permission from Elsevier.

3. PT-FREE IR-BASED CATALYSTS AND PT–IR CATALYSTS FOR THE ORR IN PEMFCS

3.1. Pt-Free Ir-Based Catalysts. Early studies of the ORR on Ir electrodes in acid media[54−56] indicated that the mechanism for oxygen reduction is most likely the same as that for Pt cathodes. Compared with Pt, however, a very poor ORR activity

dx.doi.org/10.1021/cs4011875 | ACS Catal. 2014, 4, 1426−1440

Table 1. OER Activity and Stability of Binary and Ternary IrO_2-Based Catalysts and Nanostructured IrO_2 Catalysts

catalyst	characteristics	OER activity	stability	refs
IrO_2–RuO_2	$Ir_{1-x}Ru_xO_2$ solid solution formation; surface enrichment in Ir	$RuO_2 > Ir_{1-x}Ru_xO_2 > IrO_2$	$IrO_2 > Ir_{1-x}Ru_xO_2 > RuO_2$	11–22
IrO_2–SnO_2	$Ir_{1-x}Sn_xO_2$ solid solution formation; surface enrichment in Ir	increase in the Ir-normalized OER activity with increasing Sn content up to 80% Sn	high stability	30, 38
	$Ir_{1-x}Sn_xO_2$ solid solution formation; slight surface enrichment in Sn	decrease in the OER activity of $Ir_{1-x}Sn_xO_2$ with increasing Sn content		31
	formation of two solid solutions: a SnO_2-rich phase and an IrO_2-rich phase	optimum OER activity for $IrO_2/SnO_2 = 2$		32
IrO_2–Ta_2O_5	decrease in the crystallite size compared with pure IrO_2; Ir surface enrichment in Ta_2O_5	high OER activity for IrO_2–Ta_2O_5 70–30 mol %	high stability for IrO_2–Ta_2O_5 70–30 mol %	46–51
IrO_2–SiO_2	presence of IrO_2 and SiO_2 phases; decrease in IrO_2 grain size with increasing SiO_2 content	decrease in specific activity with SiO_2 content	IrO_2–$SiO_2 > IrO_2$ for $SiO_2 \leq 50$ mol %	54–56
IrO_2–MnO_2	$Ir_xMn_{1-x}O_2$ solid solution formation for IrO_2 30 ≥ mol %	IrO_2–$MnO_2 = IrO_2$ for $IrO_2 \geq 10$ mol %	IrO_2–$MnO_2 > IrO_2$ for $MnO_2 \leq 50$ mol %; maximum stability for IrO_2 = 70 mol %	57
$Bi_2Ir_2O_7$	pyrochlore structure	$Bi_2Ir_2O_7 \sim IrO_2$	high stability	58
$(Ir_{0.25}Ru_{0.25}Sn_{0.5})O_2$	formation of a mixed (Sn, Ru, Ir)O_2 rutile phase.	IrO_2–$RuO_2 > IrO_2 > (Ir_{0.25}Ru_{0.25}Sn_{0.5})O_2$	$(Ir_{0.25}Ru_{0.25}Sn_{0.5})O_2 > IrO_2 > IrO_2$–$RuO_2$	24
$Ir_xRu_yTa_zO_2$ ($x + y + z = 1$)	increase in particle size increase with increasing Ta content	decrease in the OER activity with increasing Ta content		25
$Ir_{0.4}Ru_{0.6}Mo_xO_y$	smaller crystallite size than $Ir_{0.4}Ru_{0.6}O_2$	$Ir_{0.4}Ru_{0.6}Mo_xO_y > Ir_{0.4}Ru_{0.6}O_2$		26
$RuIrCoO_x$	presence of Ir, Ru, RuO_2, IrO_2, and Co_3O_4	$RuIrCoO_x > RuIrO_x$	high stability	27
$Sn_{0.78}Ir_{0.15}Ta_{0.07}O_{2.175}$	decrease in the crystallite size compared with IrO_2–SnO_2; Ta presence promotes surface enrichment in Ir	$Sn_{0.78}Ir_{0.15}Ta_{0.07}O_{2.175} > Sn_{0.85}Ir_{0.15}O_2$		41
$(Ir_{1-2x}Sn_xNb_x)O_2$	ternary $(Ir_{1-2x}Sn_xNb_x)O_2$ solid solution formation	$(Ir_{1-2x}Sn_xNb_x)O_2 \sim IrO_2$ up to 40 mol % IrO_2 ($x = 30$); $(Ir_{0.20}Sn_{0.40}Nb_{0.40})O_2$ only 20% lower activity than IrO_2	$(Ir_{1-2x}Sn_xNb_x)O_2 > IrO_2$	42
IrO_x–Sb_2O_5–SnO_2	metastable solid solution		IrO_x–Sb_2O_5–$SnO_2 > IrO_2$	43
$(Sn_{0.80}Ir_{0.20})O_2$/10F		$(Sn_{0.80}Ir_{0.20})O$/10F ~ IrO_2	$(Sn_{0.80}Ir_{0.20})O$/10F ≥ IrO_2	48
Ir nanodendrites	dendritic Ir with branches in various directions; single-crystalline Ir nanodendrites	$Ir_{nanodendrites} > Ir_{nanoparticles}$	$Ir_{nanodendrites} > Ir_{nanoparticles}$	49
IrO_2 nanotube arrays	IrO_2 nanostructures with a uniform tubular morphology	$IrO_{2nanotubes} > IrO_{2nanoparticles}$	$IrO_{2nanotubes} > IrO_{2nanoparticles}$	50
mesoporous IrO_2	presence of locally ordered pores	templated $IrO_2 >$ untemplated IrO_2	templated $IrO_2 >$ untemplated IrO_2	51, 52
IrO_2–Au nanoflowers		IrO_2–$Au_{nanoflowers} > IrO_{2nanoparticles}$		53

dx.doi.org/10.1021/cs4011875 | ACS Catal. 2014, 4, 1426–1440

was observed for bare Ir.[57,58] ORR kinetic current densities (at 0.8 V) on 40% Ir/C and Pt/C catalysts obtained by current−potential curves for in O_2-saturated H_2SO_4 solution at room temperature were 0.1 and 13.9 mA cm^{-2}, respectively.[58] The surface of Ir has a strong affinity for OH or O species, leading to the formation of form a surface with oxide coverage. Notwithstanding IrO_2 possess an appreciable activity for the ORR in an acidic solution,[59] the maximum power density of a single PEMFC with IrO_2 as the cathode catalyst operating a 60 °C was ∼20 mW cm^{-2},[60] a value considerably lower than that of the cell with the benchmark Pt/C (∼350 mW cm^{-2}).[61] Hovewer, the ORR activity of Ir can be increased overall by alloying with first row transition transition metals,[58,62−68] and a high methanol tolerance during ORR can be obtained by addition of metal chalcogenides to Ir.[69−73] Moreover, the ORR activity of Ir can also be increased by the inclusion of iridium in metal−organic composites.[74−76] Finally, iridium can be used as a cocatalyst by Ir decoration of binary Pt-free catalysts.[77,78]

3.1.1. Ir−M Alloy Catalysts. The effect of the addition of a second metal (M = Co,[58,62] V,[63−65] Ti,[66] and Fe[67]) on the ORR activity of Ir catalysts was investigated. Formation of IrM alloys was observed, together with the presence of M oxides. With the current density normalized by geometric area, the ORR activity of Ir−M/C catalysts was considerably higher than that of Ir/C but lower than that of Pt/C. Figure 8 shows the cell voltage as a function of current density for single PEMFCs using Ir/C (40 wt %) and Ir−V/C (40:10 wt %) as cathode electrocatalysts with a loading of 0.4 mg_{Ir} cm^{-2}.[65] The Ir−V/C (40:10 wt %) catalyst attained a maximum power density (MPD) of 517 mW cm^{-2}, only 24% lower than that of the cell with Pt/C, but ∼2.2 times higher than that of the cell with Ir/C. Considering the scarcity and cost of Ir, the effects of both a lower Ir loading in the electrode and a lower Ir/V ratio on PEMFC performance were also evaluated. High cell performances (430 and 450 mW cm^{-2}) were obtained even when the Ir loading was decreased to 0.2 mg cm^{-2} (Ir/V = 10:40 wt %) and 0.1 mg cm^{-2} (Ir/V = 5:45 wt %), respectively. The increase in the ORR activity of Ir was ascribed to IrM alloy formation, slightly enhancing the Ir lattice parameter and modifying the Ir electronic structure, thus enhancing oxygen adsorption. Moreover, because M is generally unstable in acid, the improved ORR activity can also be ascribed to the increase in th eIr surface area by M species dissolution, leaving a porous structure.

Ir−Co/C, Ir−Ni/C, and Ir−Cr/C catalysts showed higher formic acid tolerance during oxygen reduction in acid solution than both Pt/C and Pd/C.[68] Unlikely from Pt/C, the ORR pathway of Ir−M catalysts could be independent of the presence of formic. Ir−M (M = Se[69−72] and S[73]) chalcogenide electrodes were tested as ORR methanol-tolerant cathodes. The activity of iridium for methanol oxidation is very poor, making it a potentially methanol-tolerant material. However, Ir tends to form on its surface a layer of Ir oxide, which, unlike Ir metal, possesses an appreciable activity for methanol oxidation. The presence of Se/S suppresses the formation of IrO_2, making IrSe and IrS methanol-tolerant catalysts. Moreover, the addition of Se/S increases the ORR activity of Ir. In the absence of methanol, Ir−Se and Ir−S showed higher ORR activity than that of pure Ir but considerably lower than that of Pt. In the presence of methanol, instead, the ORR activity of Ir−Se and Ir−S was higher than that of Pt.

3.1.2. Ir in Metal−Organic Composites. Bouwcamp-Wijnoltz et al.[74] investigated the ORR on carbon-supported iridium chelates [iridium octaethylporphyrin (IrOEP/C), iridium tetraphenylporphyrin (IrTPP/C), and iridium phthalocyanine (IrPc/C)]. In both porphyrins, a four-electron reduction was observed. With IrPc and heat-treated porphyrins, H_2O_2 was obtained. Among pyrolyzed IrTPP, CoTPP, FeTPP, and IrOEP, the IrOEP catalyst showed the highest activity. The heat-treated metal chelates presented higher ORR activity than Ir/C. By in situ Raman spectroscopy, it was found that the ORR pathway at adsorbed layers of IrOEP, IrTPP, and IrPc depends on the type of support.[75]

With the current density normalized by geometric area, the ORR activity of a series of carbon-supported metal−polythiophene composite (M−PTh/C, M = Ir, Ru, Pd, Co, Fe, Ni, Sn) electrocatalysts was investigated under acidic conditions using rotating disk electrode (RDE) voltammetry.[76] Ir−, Ru−, and Pd−PTh/C showed much more positive ORR onset potentials than the other metal−polythiophene composites. In these three catalysts, O_2 electroreduction occurred by the four-electron reduction pathway. Considering all the electrochemical factors (onset potential, electrons transferred, and exchange current density), Ir− and Ru−PTh/C were the more effective for the ORR. As can be seen in Figure 7, the RDE voltammetry curves in an O_2-saturated H_2SO_4 solution of Ir−PTh/C were independent of the number of runs, indicating a remarkable stability. Instead, the RDE voltammetry curves of Ru− and Pd−PTh/C indicated a decrease in the ORR activity with an increase

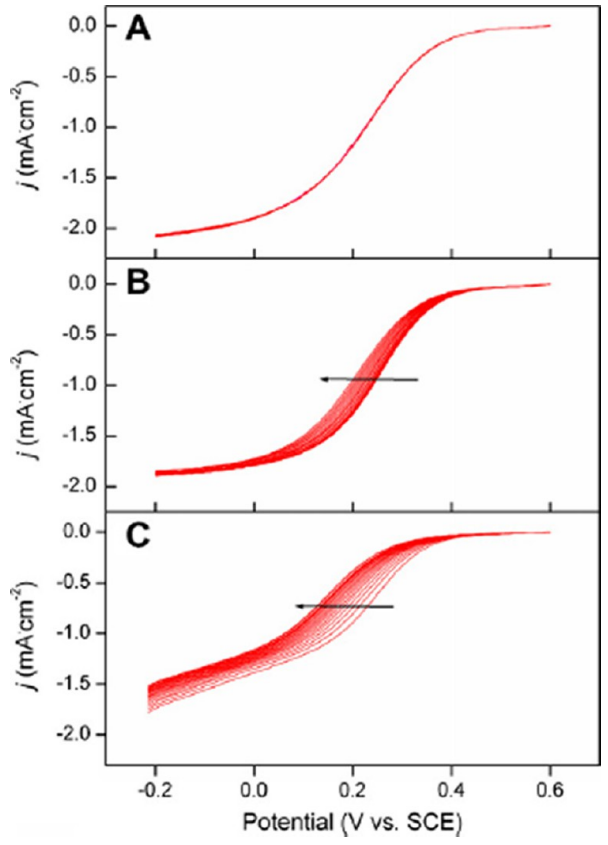

Figure 7. Rotating disk electrode (RDE) voltammograms for the ORR obtained repetitively for 20 runs in an O_2-saturated 0.5 M H_2SO_4 at M−PTh/C loaded GC electrode loaded with (A) Ir−, (B) Ru−, and (C) Pd−PTh/C (rotation speed =400 rpm; scan rate = 5 mV s^{-1}). Arrows indicate the order of RDE runs from first to 20th. Reproduced from ref 76, copyright 2011, with permission from Elsevier.

dx.doi.org/10.1021/cs4011875 | ACS Catal. 2014, 4, 1426−1440

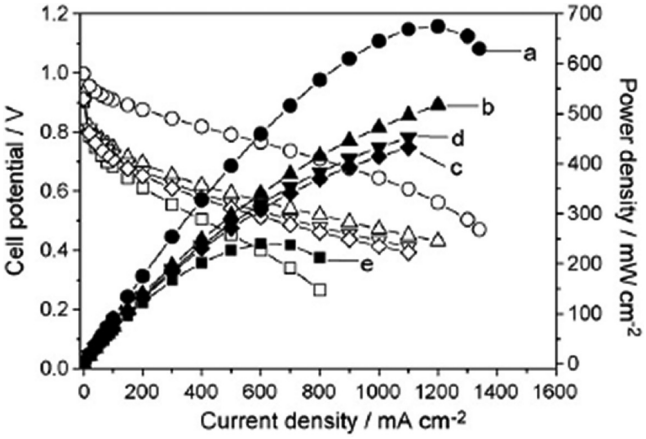

Figure 8. Cell potential and power density curves of single PEMFCs with Pt/C, Ir/C, and Ir−V/C as cathode electrocatalysts with different Ir loadings: (a) 40% Pt/C, 0.4 mg_{Pt} cm^{-2}; (b) 40% Ir−10% V/C, 0.4 mg_{Ir} cm^{-2}; (c) 10% Ir−40% V/C, 0.2 mg_{Ir} cm^{-2}; (d) 5% Ir−45% V/C, 0.1 mg_{Ir} cm^{-2}; and (e) 40% Ir/C, 0.4 mg_{Ir} cm^{-2}. Reproduced from ref 65, copyright 2009, with permission from Elsevier.

in the number of RDE runs, that is, a poor stability. However, no comparison with Pt was carried out.

3.1.3. Ir-Decorated Pt-Free Binary Catalysts. It was found that Ir decoration enhances the ORR activity of some binary catalysts. The Ir-decorated PdCu catalyst was prepared by partial surface replacement of Pd and Cu by Ir.[77] The ECSA of Ir−PdCu/C was slightly higher than that of PdCu/C. The mass activity and the performance in a single PEMFC of Ir−PdCu/C as a cathode catalyst were higher than those of PdCu/C. The higher activity of the Ir−PdCu/C catalyst was ascribed to an enhancement of both metallic component dispersion and oxygen bond cleavage by Ir atoms. The ORR of $RuSe_x$/C nanoparticles was enhanced by decoration with iridium nanoparticles in a more extended degree than the simple sum of the ORR at $RuSe_x$/C and Ir alone.[78] Ir is an effective catalyst for the reduction of H_2O_2 (rather than O_2), so the mixture of Ir with a moderate (for O_2 reduction) catalyst, such as $RuSe_x$, results in a composite catalyst with high ORR activity, also in the presence of methanol. Also for these catalysts, no comparison with Pt was performed.

3.2. Pt−Ir and Pt−Ir-Based Catalysts. *3.2.1. Pt−Ir and Pt−Ir−Co Alloy Catalysts.* The ORR activity of Pt-based and non-Pt catalysts for low-temperature fuel cells was investigated by high-throughput optical screening.[79] The results indicated that Pt−Ir possess higher activity and methanol tolerance than pure Pt. Moreover, an acceptable stability at high potential in acid environment makes Pt−Ir a potential PEMFC cathode catalyst. Thus, the ORR activity of Pt−Ir catalysts has been extensively investigated.[80−85] Generally, a positive effect of Ir addition on the ORR activity of Pt has been observed.[80−84] The higher ORR activity of Pt−Ir alloy catalysts than that of Pt alone was ascribed mainly to geometric factors (decrease in the Pt−Pt bond distance) or electronic factors (increase in the Pt d electron vacancy). Moreover, Ir has a strong affinity to OH adsorption. Thus, the formation of $Ir-OH_{ads}$ starts at more negative potentials than $Pt-OH_{ads}$.

Potentiodynamic polarization curves of cosputtered alloyed Pt−Ir films with different Pt/Ir atomic ratios in oxygen-saturated H_2SO_4 solution were recorded at room temperature by Topalov et al.[80] The same measurements were carried on carbon-supported Pt and Ir catalysts by Yang et al.[58] To compare the ORR specific activity (expressed as the current density at 0.8−0.825 V) of cosputtered films and carbon supported catalysts, the current density of Pt−Ir and Ir catalysts was divided by the corresponding current density of Pt. The Pt−Ir-to-Pt ORR activity ratio (A_{PtIr}/A_{Pt}) on Ir content in the catalyst by the different data sets is shown in Table 2. In agreement with the literature data (it is known that both the geometric and electronic effects of alloying on ORR activity obey to a volcano-type curve[86,87]), the ORR activity of the Pt−Ir catalysts went through a maximum, and among the various catalysts, the Pt−Ir (85−15) catalyst presented the highest specific activity. The A_{PtIr}/A_{Pt} ratio of all the binary catalysts ($A_{PtIr}/A_{Pt} > 1$) was higher than that of Pt ($A_{PtIr}/A_{Pt} = 1$) and considerably higher than that of Ir ($A_{PtIr}/A_{Pt} = 0.007$).

Table 2. Pt−Ir-to-Pt ORR Specific Activity Ratio (A_{PtIr}/A_{Pt})[a] of Cosputtered Pt and Pt−Ir Films[80] and Carbon-Supported Pt and Ir Catalysts[58]

sample	type of catalyst	A_{PtIr}/A_{Pt}
Pt	cosputtered films	1
Pt−Ir (94:6)		2.9
Pt−Ir (89:11)		6.1
Pt−Ir (83:17)		4.7
Pt−Ir (80:20)		3.6
Pt−Ir (61:39)		1.3
Pt	carbon-supported catalysts	1
Ir		0.007

[a]Expressed as current density at 0.8−0.825 V from potentiodynamic polarization curves in oxygen-saturated 0.5 M H_2SO_4 solution at room temperature.

Liu et al.[83] ascribed the positive effect of the Ir presence to the higher surface area, but not to an increased specific activity. Huang et al.[85] instead observed a slightly negative effect of the Ir presence on the ORR activity of Pt, increasing with the increases in the Ir content in the Pt−Ir catalysts. The different results regarding the ORR activity should be attributed to different alloying degrees. Indeed, when an increase in the specific activity was observed, formation of alloyed Pt−Ir catalysts was also reported.[80−84] Instead, the Pt−Ir catalysts prepared by Huang et al.[85] consisted of a physical mixture of Pt/TiO_2 and Ir/TiO_2, clearly in a nonalloyed form. In the same way, the Pt−Ir catalysts prepared by Liu et al.,[80] formed by alternating layers of Pt and Ir, were nonalloyed. Loukrakpam et al.[88,89] investigated the ORR activity of Pt−Ir−Co/C alloy catalysts. They observed that the specific activity of ternary catalysts was higher than that of Pt/C. The ORR activity increased with a decrease in the lattice parameter of the Pt-based alloy. A dependence of the specific activity on atomic ordering in Pt−Ir−Co alloy was found.

3.2.2. Pt Monolayer on Ir−M with and without an Pd Interlayer. Among different catalyst structures, platinum monolayer (Pt_{ML}) electrocatalysts present the highest Pt utilization. They are formed by a monolayer of Pt on carbon-supported metal or metal−alloy nanoparticles.[90] Pt_{ML} are prepared by the galvanic displacement of a Cu monolayer by Pt.[91] The interaction between the Pt_{ML} and the substrate material induces a synergistic effect for ORR kinetics. Density functional theory (DFT) calculations showed that the binding energies and reactivity of small atom or molecule adsorption on strained surfaces and metal overlayers correlate well with the position of the d band center of surface atoms.[92] The ORR activity strongly depends on the d band center of Pt_{ML}. Among transition metals, iridium possesses one of the highest stabilities, similar to that of

dx.doi.org/10.1021/cs4011875 | ACS Catal. 2014, 4, 1426−1440

Pt; however, bare Ir is not a suitable support for a Pt_{ML} because it causes a remarkable decrease in the d band center owing to a high contraction of Pt lattice. As a consequence, a weak adsorption of O_2 on Pt and, hence, a low ORR activity, take place.[93]

There are essentially three ways to decrease the effect of Ir on the d band center of a Pt_{ML}: the use of (1) a Pd interlayer, (2) a PdIr sublayer, or (3) a core−shell M@Ir support. The presence of a maximum in the curve correlating the kinetic current density on Pt monolayers on six different single crystal surfaces with the calculated d band center of the Pt was observed.[94] The maximum of the curve was related to the Pt_{ML} on a Pd(111) surface. On this basis, high ORR activity catalysts were tailored, which consisted of a less expensive and more stable IrM core (M = Co, Re), a Pd interlayer, and a surface Pt_{ML}.[93,94] For both the IrCo and Ir_3Co cores, the Pd interlayer remarkably increases the ORR compared with the electrocatalyst without a Pd interlayer (Figure 9).[93] In addition to the Pd interlayer, DFT calculations showed that the molar ratio of Ir to M affects the binding strength of adsorbed OH and, thereby, the ORR activity of the catalysts.[93,94]

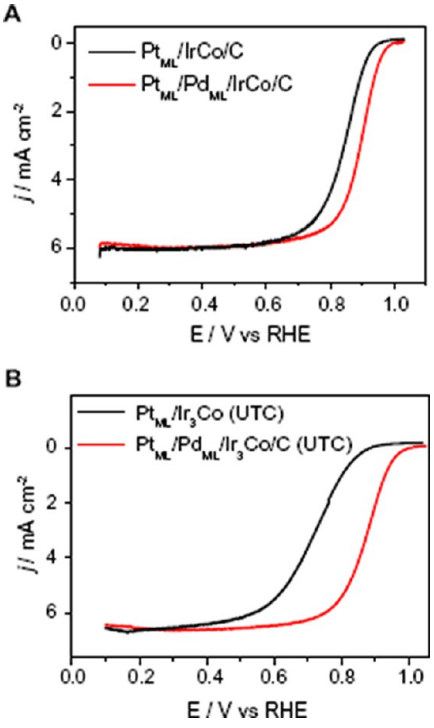

Figure 9. RDE voltammograms of Pt_{ML}/IrCo/C (A) and Pt_{ML}/Ir_3Co/C (B) with and without a Pd interlayer for the ORR in oxygen saturated 0.1 M $HClO_4$. Scan rate, 10 mV s^{-1}; rotating speed, 1600 rpm. Reproduced from ref 93, copyright 2010, with permission from Elsevier.

The best results were obtained with the Pt_{ML}/Pd_{ML}/Ir_2Re and Pt_{ML}/Pd_{ML}/IrCo electrocatalysts. By DFT calculations, it was found that, in Pt_{ML}/IrCo, that is, without the Pd interlayer, Ir and Co may segregate from the core to the surface, considerably weakening the stability of the structure. In Pt_{ML}/Pd_{ML}/IrCo, instead, the Pd interlayer inhibits the segregation of the core elements.[95] The second method way is based on a PdIr sublayer.[96] The ORR kinetics was investigated in acid solutions on Pt_{ML} deposited on modified carbon-supported PdIr nanoparticles. To enhance the Pd stability under fuel cell operating conditions, Ir was introduced into the Pd substrate. The ORR activity on Pt_{ML}/PdIr/C was enhanced in comparison with that on Pt/C and Pt_{ML}/Pd/C as a result of a ligand effect on the Pt surface by the presence of PdIr in the catalyst sublayer and a higher compression of the Pt_{ML} on PdIr/C than on Pd/C.

Finally, a Pt_{ML} was deposited on the surface of carbon-supported nonnoble metal/noble metal core−shell nanoparticles by galvanic displacement of a Cu monolayer with Pt. The use of nonnoble metals for the cores results in a further reduction of the content of the noble metal in the electrocatalysts. The noble metal shell in the core−shell nanoparticle protects the nonnoble core from the acid electrolyte, preventing its dissolution, and improves the catalytic properties of a Pt_{ML} by affecting its electronic properties or by inducing strain in the monolayer. Ir was chosen as the noble metal, and Fe and Ni, as the nonnoble metal of the core−shell strucuture.[97,98] A higher activity and stability of Pt_{ML} on M@Ir (M = Ni, Fe) than that of Pt_{ML}/Ir/C and Pt/C were observed.[97,98]

3.2.3. Stability and Durability of Ir, Pt−Ir and Pt−Ir-Based Catalysts for the ORR. The stabilities of Pt atoms and other transition metal atoms (Ir, Pd, Rh, Ni, and Co) toward the ORR in an acid medium was investigated by DFT studies.[99] Iridium was the most stable among the various pure metals in comparison wtih Pt. Most of the metals alloyed with Pt caused a decrease in the Pt stability against dissolution. On the other hand, among the different PtM alloys, the PtIr alloy was the most stable, with Ir more stable than Pt. On the other hand, the stability of a series of Pt-based catalysts was evaluated by performing a high-throughput screening.[100] The screening result indicated that Pt−Ir (44:56) lost nearly all its activity. The different results on the stability of Pt−Ir catalysts in acid medium could depend on the different alloying degrees. Pt−Ir−Co (50:25:25) and Pt−Ir−Cr (50:25:25) ternary alloys were studied using DFT and compared with the bimetallic Pt−Co (75:25) and Pt−Cr (75:25) alloys to determine the effect of the substitution of Pt by Ir on the electrochemical stability of the Pt atoms.[101] Ternary alloys exhibit a strong Pt surface segregation tendency, leading to the formation of a Pt monolayer on their surfaces. The Pt skin surfaces of Pt−Ir−Co and Pt−Ir−Cr show an enhanced electrochemical stability with respect to the dissolution of Pt atoms from the alloy surface. The stability of Pt, Pt−Co, and Pt−Ir−Co catalysts was tested in a fuel cell by repetitive potential cycling (RPC) between 0.87 and 1.05 V vs SHE at 120 °C in the absence of O_2.[102] Pt and Pt−Co cathodes showed severe ECSA degradation, with about 50% of initial ECSA lost after 2200 cycles. The Pt−Ir−Co cathode, instead, showed very little degradation after a similar number of cycles. The stability of Pt−Ir−Co catalysts, however, depends on the amount of Ir in these compounds. The low Ir content in Pt−Ir−Co (67:8:25) resulted in Co loss and in a decrease in the ORR activity following RPC.[103]

The stability of Pt and Pt on Ir was examined as cathode catalysts in a single cell PEMFC.[104] Pt was deposited on metallic layers of Ir, the thickness varying between 1.5 and 20 nm. For thin layers of Ir, the initial ORR activity was equal to or superior to that of bare Pt, but for thicker Ir films, it was lower. All Ir-containing catalysts showed an increased stability compared to bare Pt during RPC between 0.6 and 1.2 V vs RHE.

3.2.4. Corrosion Reduction of ORR Catalyst Carbon Support by the Addition of Ir-Based Catalysts to the Catalyst Layer. High surface area carbon is commonly used as a PEMFC catalyst support.[28] Because carbon has a low equilibrium potential for carbon corrosion, it is thermodynamically unstable above the equilibrium potential, as shown in eqs 11 and 12. Insignificant carbon oxidation occurs during the normal PEMFC operation; however, carbon corrosion can occur at potentials higher than

dx.doi.org/10.1021/cs4011875 | ACS Catal. 2014, 4, 1426−1440

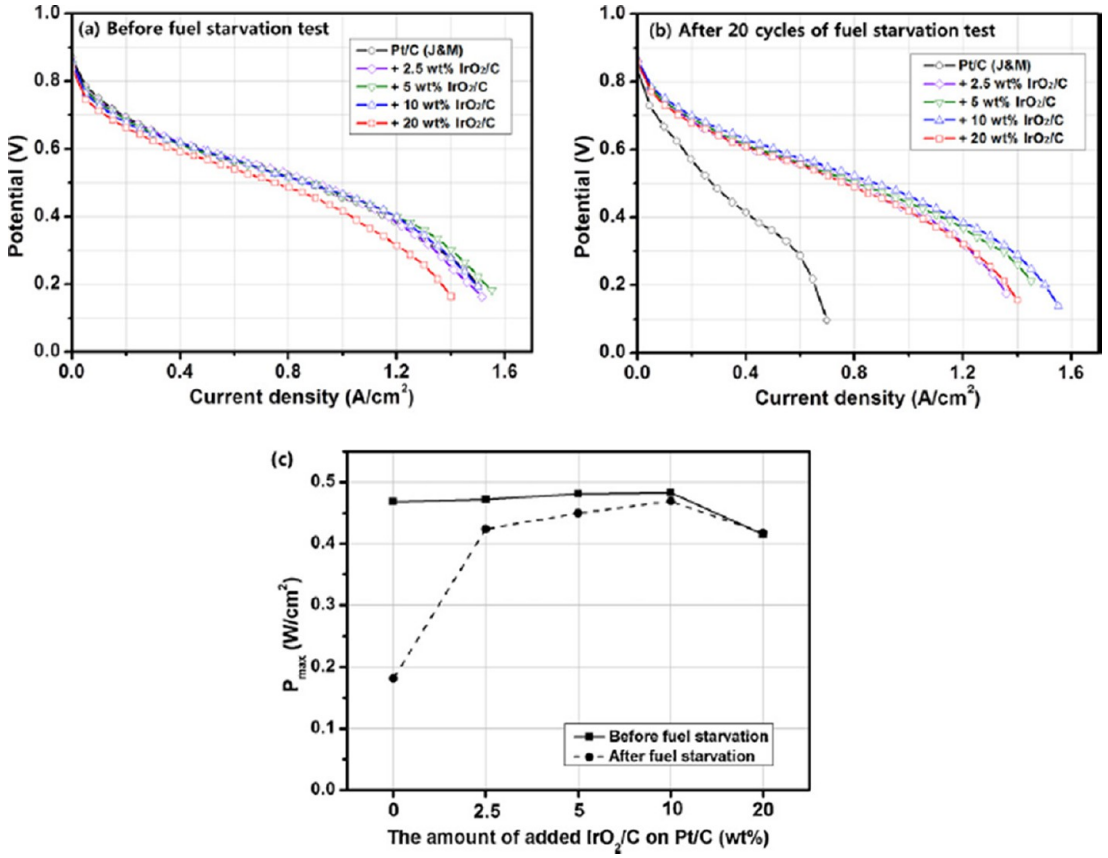

Figure 10. Comparison of the single cell performance (a) before and (b) after 20 cycles of the accelerated fuel starvation test. (c) Comparison of the maximum power density (P_{max}). Cell performance test: 70 °C, 1 atm; anode gas, H_2 (200 ccm); cathode gas, air (650 ccm). Reproduced from ref 29, copyright 2013, with permission from Elsevier.

Table 3. ORR Activity and Stability of Binary and Ternary Ir-Containing Catalysts

	catalyst	ORR activity	stability	refs
Pt-free	Ir−M alloys (M = Co, V, Ti, Fe)	Pt/C > Ir−M/C > Ir/C; Ir−M/C > Pt/C (in HCOOH presence)		58, 62−68
	Ir−M chalcogenides (M = Se, S)	Pt/C > Ir−M/C > Ir/C; Ir−M/C > Pt/C (in CH_3OH presence)		69−73
	Ir chelates	pyrolyzed IrOEP > IrTPP, CoTPP, FeTPP		74, 75
	Ir polythiophene	Ir−PTh/ ∼ Ru−Th > Co−, Fe−, Ni−, Sn−PTh/C	Ir−PTh/C > Ru−, Pd−PTh/C	76
	Ir-decorated PdCu/C and $RuSe_x$/C	Ir−PdCu/C > PdCu/C Ir−$RuSe_x$/C > $RuSe_x$/C		77, 78
Pt-based	Pt−Ir alloys	Pt−Ir > Pt	Pt−Ir > Pt	79−84
	Pt−Ir−M (M = Co,Cr)	Pt−Ir−M > Pt	Pt−Ir−M > Pt−M	88, 89, 101−103
	Pt monolayer on Pd/Ir−M (M = Co, Re)	Pt_{ML}/Pd/Ir−M > Pt_{ML}/Ir−M		93−95
	Pt monolayer on PdIr	Pt_{ML}/PdIr/C > Pt_{ML}/Pd/C > Pt/C		96
	Pt monolayer on M@Ir (M = Fe, Ni)	Pt_{ML}/M@Ir/C > Pt_{ML}/Ir/C > Pt/C	Pt_{ML}/M@Ir/C > Pt/C	97, 98
	Pt/Ir	Pt/Ir > Pt	Pt/Ir > Pt	104

the open circuit potential (OCP). As the cathode potential increases to as much as twice the OCP during fuel starvation, cathode carbon support corrosion takes place. Electrochemical corrosion of the carbon support causes the sintering and agglomeration of Pt particles, resulting in a decrease in the ECSA of the catalyst. The presence of IrO_2 or RuO_2 can be a suitable method for preventing corrosion of the carbon support because the OER is more electrochemically feasible than carbon oxidation. As a result, IrO_2 or RuO_2 can remove water from the catalyst layer; however, the use of these materials on the cathode can have an adverse effect on the ORR by covering the active surface area of the catalyst.

The addition of IrO_2 and IrO_2/C to Pt/C was investigated to determine their effect on the performance and durability of PEMFCs under fuel starvation conditions.[29] Although the addition of IrO_2 to the cathode catalyst resulted in improved durability, it had an adverse effect on the PEMFC performance by a screening effect on the Pt/C. The cell performance under normal operation was decreased severely by 35% by adding 10 wt % IrO_2 to Pt/C. Conversely, as shown in Figure 10a, before the fuel starvation test, the initial performance of the cell using the Pt/C−10 wt % IrO_2/C cathode catalysts was comparable to that of the cell only using Pt/C. On the other hand, Pt/C−20 wt % IrO_2/C showed evident performance loss, a 14% loss of the

dx.doi.org/10.1021/cs4011875 | ACS Catal. 2014, 4, 1426−1440

maximum power density (Figure 10c). An accelerated fuel starvation test was carried out to examine the performance variation of PEMFCs using different amounts of IrO_2/C. Figure 10b shows the current−potential curves after 20 cycles of the fuel starvation test. The peak power density of the cell using the Pt/C alone decreased drastically by 61.31%. On the other hand, the performance of the cell with Pt/C plus 2.5, 5, 10, and 20 wt % IrO_2/C decreased by 10.21, 6.52, 2.93, and 0.0%, respectively. The addition of IrO_2/C to Pt/C helps to maintain a constant cell performance under harsh fuel starvation conditions. As the amount of IrO_2/C increased, the cell showed enhanced durability because water molecules in the catalyst are decomposed more rapidly. The results of the cell performance indicated that the optimum IrO_2/C amount is 10 wt % in the cathode catalyst. In the same way, the addition of 1 wt % Ir dendrite (0.008 mg cm^{-2}) to the cathode catalyst layer decreased the electrochemical carbon corrosion by 84% at 1.6 V vs NHE compared with a conventional MEA.[105]

The ORR activity and stability of binary and ternary IrO_2-based catalysts and nanostructured IrO_2 catalysts are summarized in Table 3.

4. PT/IR CATALYSTS FOR OER/ORR IN URFCS

4.1. Bifunctional Oxygen Catalysts (BOC). A Unitized regenerative fuel cell is an effective way for producing hydrogen and clean energy. A URFC splits water by electrolysis, stores the hydrogen gas, and produces electricity by the fuel cell process.[106] Nevertheless, to combine a PEMWE and a PEMFC is still a big challenge. The oxygen reduction and the water oxidation are the limiting reaction steps at the oxygen electrode for PEMFC or PEMWE, respectively. Therefore, its high efficiency depends on the type of electrocatalysts and the capability of the oxygen electrode to operate under the PEMFC or PEMWE conditions. So broad research is focused on developing a new design for the oxygen electrode in URFCs. Generally, the preferred ORR catalysts (Pt and Pt alloys) demonstrate poor OER performance, and the preferred OER catalysts (IrO_2 and RuO_2) demonstrate poor ORR performance. From a screening of combinations of five elements (Pt, Ru, Os, Ir, and Rh) as oxygen reduction and water oxidation catalysts, Pt−Ru−Ir ternary catalysts with low Ir content were found to be the most effective.[107] As can be seen in Figure 11, $Pt_{4.5}Ru_4Ir_{0.5}$ and Pt−Ir have similar OER activity, but Pt−Ir is poor for the ORR; in the same way, $Pt_{4.5}Ru_4Ir_{0.5}$ and Pt have similar ORR activity, but Pt is poor for the OER. Only $Pt_{4.5}Ru_4Ir_{0.5}$ has the highest activity in both modes. Yim et al.[108] prepared and tested several electrocatalysts, including both fuel cell and water electrolysis, in a single URFC system. In contrast to the previous results, the catalysts revealed fuel cell performance in the order of Pt black > Pt−Ir > Pt−RuO_x > Pt−Ru ∼ Pt−Ru−Ir > Pt−IrO_x and water electrolysis performance in the order of Pt−Ir ∼ Pt−IrO_x > Pt−Ru > Pt−Ru−Ir > Pt−RuO_x ∼ Pt black. Considering both results, Pt−Ir showed the best URFC performance.

4.2. Bifunctional Pt−IrO_2 and Pt−Ir Catalysts. *4.2.1. Conventional Pt−IrO_2 and Pt−Ir Catalysts.* Most of the works on bifunctional oxygen catalysts (BOC) for the URFCs were addressed with few exceptions (ternary Pt−RuO_2−IrO_2[109] and Pt−Ru−Ir[110] catalysts) to binary Pt−IrO_2[111−123] and Pt−Ir[124−130] catalysts. The first BOCs were a physical mixture of unsupported Pt blacks and IrO_2[111−113] or Ir blacks.[124,125,127] Both of them, however, were not very well dispersed in the solvent, resulting in poor interdispersion of the two kinds of catalysts and low bifunctional performance. To overcome this problem, Pt blacks[114] or, more commonly, IrO_2[115,116,119,123] were utilized as the support, with the other catalyst deposited on the support (IrO_2/Pt or Pt/IrO_2, respectively). Generally, the ORR activity was expressed with the current density normalized by Pt mass, whereas the OER activity wasd expressed with the current density normalized by catalyst mass. Ioroi et al.[114] observed that the URFC with IrO_2/Pt (20 at% Ir) showed a fuel cell performance similar to that with the mixed IrO_2−Pt electrode of higher Pt content (10 at% Ir) while maintaining water electrolysis performance. Pt/IrO_2 generally performed better as a URFC catalyst than the mixed catalyst.[115,116,119] Different effects, however, were observed. Yao et al.[115] found that Pt/IrO_2 has slightly lower ORR activity but markedly higher OER activity than mixed IrO_2−Pt. Conversely, Zhang et al.[116] and Cruz et al.[119] observed for water electrolysis nearly the same performance, but for oxygen reduction, a better performance of Pt/IrO_2 than the mixed catalyst may be due to a lower dispersion of this catalyst compared with supported Pt.

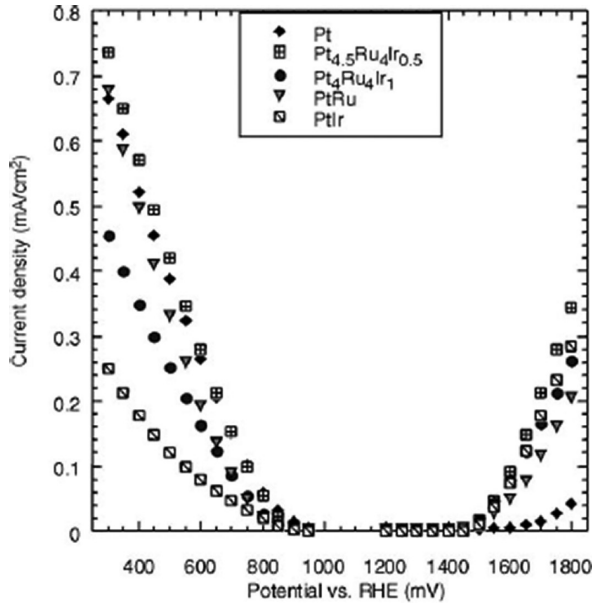

Figure 11. Polarization curves of the oxygen electrode in electrolysis (oxygen evolution) and fuel cell (oxygen reduction) modes for the indicated catalysts. Reproduced from ref 107, copyright 2001, with permission from Elsevier.

4.2.2. Pt−IrO_2−Ir Catalysts with Improved Electronic Conductivity. The ORR activity of Pt/IrO_2 catalysts can be affected by their low conductivity, as a result of their formation of IrO_2 agglomerates with higher ohmic resistance hindering the electronic paths between the Pt particles. To increase the conductivity of IrO_2, Ir nanoparticles were added to IrO_2 by two ways: (i) by mixing Ir and IrO_2[120] and (ii) by depositing metallic Ir nanoparticles on the IrO_2 surface.[122] $Ir_x(IrO_2)_{1-x}$ ($x < 1$) supports with varying Ir and IrO_2 were prepared using the Adams fusion method.[120] The Pt/$Ir_{0.3}(IrO_2)_{0.7}$ catalyst showed the highest ECSA and the highest ORR activity and excellent OER activity. The enhanced performance of Pt/$Ir_{0.3}(IrO_2)_{0.7}$ catalyst was ascribed to the introduction of Ir into the IrO_2 support, improving the electronic conductivity. Ir nanoparticles were deposited on the IrO_2 surface by a microwave-assisted polyol process, and the resulting IrO_2@Ir was used as a support for Pt (Scheme 1).[122] The ORR activity of Pt/IrO_2@Ir was higher than that of Pt/IrO_2, and their OER activities were comparable. The structure of Pt/IrO_2@Ir also increases platinum stability, because

dx.doi.org/10.1021/cs4011875 | ACS Catal. 2014, 4, 1426−1440

Scheme 1. Schematic Diagram of Pt/IrO_2@Ir Catalyst Structure[a]

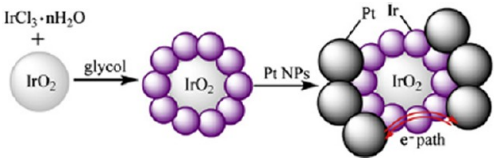

[a]Reproduced from ref 122, copyright 2012, with permission from Elsevier.

the interaction between Pt and Ir nanoparticles can successfully avoid Pt agglomeration. However, unlike carbon black, neither Pt or IrO_2 is a satisfactory support to obtain highly dispersed particles for high catalyst loading. For this reason, to increase the surface area of the substrate, nanostructured IrO_2 and Ir and ceramic materials have been investigated as supports for BOCs.

4.2.3. Pt Supported on Nanostructured IrO_2 and Ir. To increase the active surface area, Pt was deposited on porous IrO_2.[123] Porous IrO_2 provides internal and external sites for Pt deposition. Pt supported on porous IrO_2 showed both a higher OER activity and a higher ORR activity than Pt supported on conventional IrO_2.

A novel, interesting nanodendritic Ir@Pt bifunctional electrocatalyst was prepared by a one-pot synthesis method.[129] The Ir nanodendrites are well dispersed and their mean size (15 nm, Figure 12a) is considerably smaller than that of Ir blacks (inset of Figure 12d). The TEM image in Figure 12b shows the dendritic nanostructure of Ir_{67}@Pt_{33}. The lattice fringes in the HRTEM image (inset in Figure 12b) indicate good crystallinity of the Ir_{67}@Pt_{33}. HAADF–STEM–EDX analysis (Figure 12c) reveals

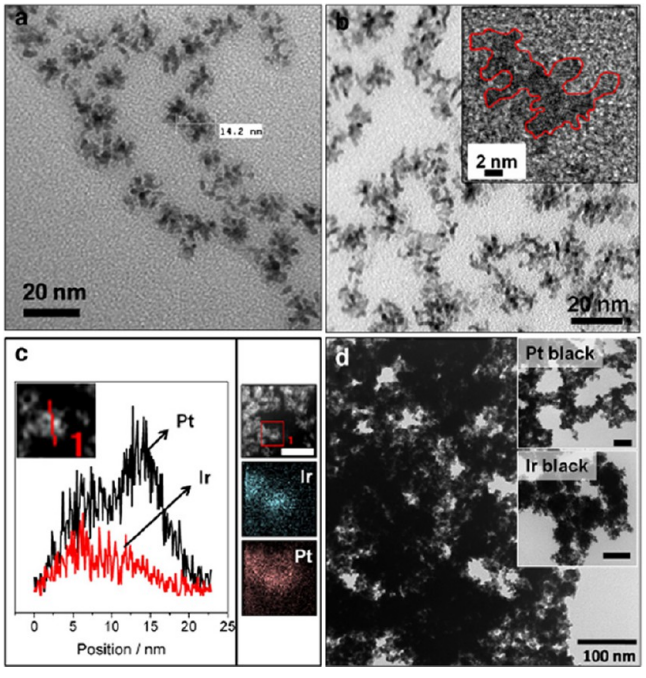

Figure 12. (a) TEM image of Ir nanodendrites. (b) TEM and (inset) HRTEM images of Ir_{67}@Pt_{33} nanodendrites. (c) High-angle annular dark field scanning transmission electron microscopy (HAADF–STEM) image and elemental maps and line profiles of Ir_{67}@Pt_{33}. (d) TEM images of $Ir_{57}Pt_{43}$ and (inset) Pt and Ir blacks. The scale bars unmarked are 50 nm. Reproduced from ref 129, copyright 2012, with permission from Elsevier.

that Pt is deposited on the surface of Ir. Conversely, large agglomerates of Pt or Ir are present in mixed $Ir_{57}Pt_{43}$ (Figure 12d). The Ir@Pt electrocatalysts showed a remarkable enhancement in the ORR and OER activities compared with the Ir and Pt mixture, ascribed to the better dispersion of Pt, the interaction between Pt and Ir, and the morphology of Ir@Pt nanodendrites.

4.2.4. Pt–IrO_2 and Pt–Ir Catalysts Supported on Ceramic Materials. Different ceramic materials were investigated as supports for Pt, IrO_2, and Ir.[117,121,128,130] Two kinds of these supported BOCs were reported: (1) Pt and IrO_2 or Ir separately supported on the ceramic material, then mixed with each other,[117,128] and (2) Pt and IrO_2 or Ir first mixed, then the mixture deposited on the support.[121,130] Titanium-based materials (TiO_2, TiC and TiCN) were investigated as a support for URFC catalysts.[117,128,130] Physical mixtures of Pt/TiO_2 and Ir/TiO_2 electrocatalysts with Pt/Ir compositions in the range from 100:0 to 70:30 were tested as BOCs.[128] Among different compositions, the Pt–Ir (85:15) catalyst showed the highest ORR and OER activities. TiO_2 support provided a high surface area for uniform dispersion of the catalyst particles, in this way increasing the URFC performance.

The ORR and OER activities of Pt–IrO_2 and Pt–Ir catalysts for URFCS are summarized in Table 4.

Altmann et al.[118] investigated various URFC oxygen electrode designs with Pt and IrO_2 catalysts. The various options, shown in Figure 13, are the following: mixture of Pt and IrO_2 (option 1), bilayer electrode formed by a layer of Pt for the fuel cell mode and a layer of IrO_2 for the electrolysis mode, (option 2), and segmented electrode (option 3). Figure 14 shows the best-performing curves for the three electrode options. A poor performance resulte in both modes when using option 3. The better performance in fuel cell mode and in electrolysis mode were shown by options 2 and 1, respectively. Considering both fuel cell and electrolysis modes, option 1 was the more effective; however, the performance of multilayer electrodes can be improved by increasing the Nafion content in the internal layer and the porosity in the external layer of the electrode.

CONCLUSIONS

Iridium and iridium-based materials have been investigated as a catalyst and cocatalyst for both OER and ORR in acid medium.

Iridium oxide is a good electrocatalyst for oxygen evolution, but the use of pure IrO_2 is limited by high costs and a short electrode lifetime, so to reduce the cost and increase the durability, mixtures of IrO_2 with a less expensive oxide, particularly SnO_2, have been intensively investigated. On the other hand, the addition of RuO_2 to IrO_2 combines the useful properties (high activity of RuO_2 and high stability of IrO_2) of both components. Binary Ir–Ru and Ir–Sn and ternary Ir–Ru–M and Ir–Sn–M oxide catalysts showed higher OER activity and stability than conventional bare IrO_2.

The activity for oxygen reduction of iridium alone as well as the activity of the oxide layer formed on the Ir surface is considerably lower than that of Pt. However, the addition of a second metal significantly increases the ORR activity of Pt. In particular, the performance of a single PEMFC with Ir–V/C as cathode catalyst was only 24% lower than that of the cell with Pt/C.

Addition of Ir to Pt increases the ORR activity of Pt. The ORR activity of alloyed Pt–Ir catalysts with different compositions was higher than that of Pt and considerably higher than that of Ir. Among various compositions, the alloyed Pt–Ir (85:15) catalyst presented the highest active area and the highest specific activity.

dx.doi.org/10.1021/cs4011875 | ACS Catal. 2014, 4, 1426–1440

Table 4. ORR and OER Activities of Pt−IrO_2 and Pt−Ir Catalysts for URFCS

catalyst	structure	OER activity	ORR activity	optimum composition	refs
Pt−IrO_2	usupported mixed Pt−IrO_2	Pt−RuO_2 > Pt−IrO_2 > Pt	Pt ≥ Pt−IrO_2 > Pt−RuO_2	IrO_2 10−30 mol %	111−113
	IrO_2/Pt	IrO_2/Pt ∼ mix Pt−IrO_2	IrO_2/Pt > mix Pt−IrO_2	IrO_2 20 mol %	114
	Pt/IrO_2	Pt/IrO_2 > mix Pt−IrO_2	Pt/IrO_2t ≤ mix Pt−IrO_2		115
		Pt/IrO_2 = mix Pt−IrO_2	Pt/IrO_2t > mix Pt−IrO_2		116, 119
	Pt/$Ir_x(IrO_2)_{1-x}$			x = 0.3	120
	Pt/IrO_2@Ir	Pt/IrO_2@Ir = Pt/IrO_2	Pt/IrO_2@Ir > Pt/IrO_2		122
	Pt/porous IrO_2	Pt/porIrO_2 > Pt/IrO_2	Pt/porIrO_2 > Pt/IrO_2		123
	Pt−IrO_2/TiO_2	high activity	high activity		117
	Pt−IrO_2/ATO	high activity	low activity		121
Pt−Ir	usupported mixed Pt−Ir	Pt−Ir ∼ Pt−IrO_x > Pt−RuO_x ∼ Pt	Pt > Pt−Ir > Pt−RuO_x	Ir 10−15 at %	124−126
	Pt−Ir/TiO_2	Pt−Ir/TiO_2 > Pt−Ir	Pt−Ir/TiO_2 > Pt−Ir		128
	dendritic Ir@Pt	Ir@Pt > Pt−Ir	Ir@Pt > Pt−Ir		129

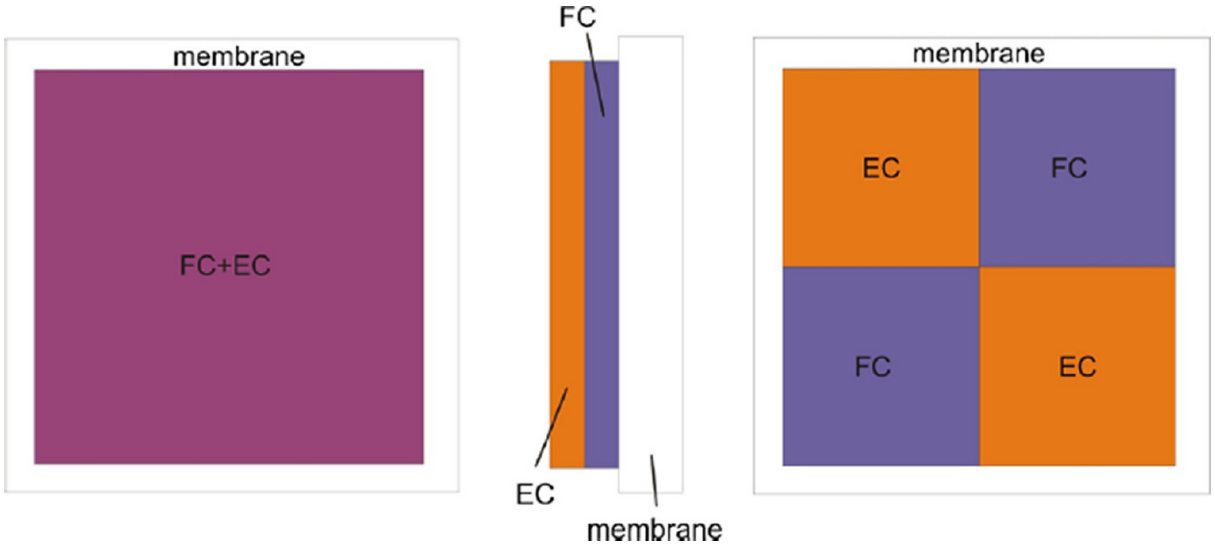

Figure 13. Oxygen electrode configurations (left, option 1, a mixture of both catalysts; middle, option 2, bilayer electrode; right, option 3, segmented electrode). Reproduced from ref 118, copyright 2011, with permission from Elsevier.

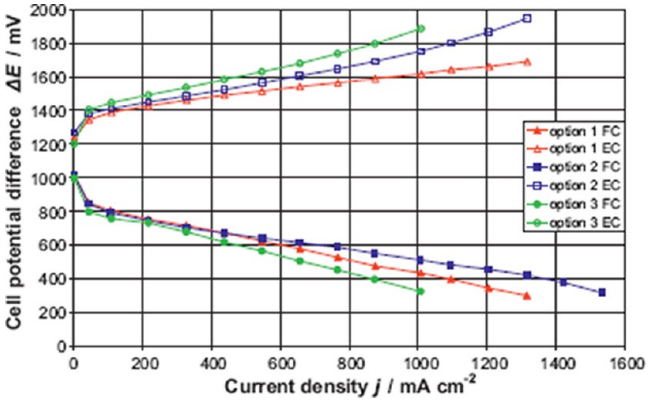

Figure 14. Cell potential difference curves of best performing membrane electrode assemblies (MEAs) in the fuel cell and the electrolysis modes for the different electrode configurations (fuel cell mode, cell temperature 85 °C, ambient pressure, gases fully humidified, hydrogen flow 0.4 l min^{-1}, oxygen flow 0.4 l min^{-1}; electrolysis mode, cell temperature 95 °C, ambient pressure, no flows). Reproduced from ref 118, copyright 2011, with permission from Elsevier.

Pure Ir is not a suitable substrate for a Pt_{ML} because oxygen is weakly adsorbed on PtML/Ir. However, the negative effect of Ir on the d band center of a Pt_{ML} can be reduced by the use of a Pd interlayer, a PdIr sublayer, or a core−shell M@Ir support. All these structures presented a higher ORR activity compared with pure Pt/C and PtML/Ir/C electrocatalysts.

The presence of Ir increases the stability of Pt, PtM alloys, and Pt_{ML} for ORR. Moreover, the presence of Ir increases the stability of the carbon support. In view of the scarcity and cost of Ir, the use of catalysts with low Ir content, such as Ir−Ru−M and Ir−Sn−M ternary oxide catalysts for the OER and Pt−Ir alloy and M@Ir supported Pt monolayer catalysts for the ORR, is strongly recommended.

A general consensus on the use of binary Pt−Ir catalysts, with Ir either in the metal or, particularly, in the oxide form, as bifunctional oxygen catalysts is reported. However, the ORR activity of Pt/IrO_2 catalysts can be affected by their low conductivity and low surface area. The low conductivity of Pt/IrO_2 catalysts is due to the formation of IrO_2 agglomerates with higher ohmic resistance, hindering the electronic paths between Pt particles. To increase the conductivity of IrO_2, Ir nanoparticles were added to IrO_2. On the other hand, unlike carbon black, neither Pt or IrO_2 is a satisfactory support to obtain highly dispersed particles for high catalyst loading. For this reason, to increase the surface area of the substrate, nanostructured IrO_2 and Ir and ceramic materials, such as titanium-based materials, have been investigated with good results as supports for BOCs.

Regarding the electrode structure, the more effective is the electrode that is formed by a mixture of Pt and IrO; however, an

dx.doi.org/10.1021/cs4011875 | ACS Catal. 2014, 4, 1426−1440

improvement in the performance of the bilayer electrodes formed by a Pt layer (fuel cell mode) and a IrO_2 layer (electrolysis mode) can be achieved by increasing the electronic conductivity and mass transport of the layers.

AUTHOR INFORMATION

Corresponding Author

*E-mail: ermantol@libero.it.

Notes

The authors declare no competing financial interest.

REFERENCES

(1) Antolini, E. *J. Appl. Electrochem.* **2004**, *24*, 563−576.
(2) Carmo, M.; Fritz, D. L.; Mergel, I.; Stolten, D. *Int. J. Hydrogen Energy* **2013**, *38*, 4901−4934.
(3) Shi, Z.; Zhang, J.; Liu, Z.-S.; Wang, H.; Wilkinson, D. P. *Electrochim. Acta* **2006**, *51*, 1905−1916.
(4) Damjanovic, A.; Brusic, V. *Electrochim. Acta* **1967**, *12*, 615−628.
(5) De Faria, L. A.; Boodts, J. F. C.; Trasatti, S. *J. Appl. Electrochem.* **1996**, *26*, 1195−1199.
(6) Da Silva, L. M.; Boodts, J. F. C.; De Faria, L. A. *Electrochim. Acta* **2001**, *46*, 1369−1375.
(7) Miles, M. H.; Klaus, E. A.; Gunn, B. P.; Locker, J. R.; Serafin, W. E.; Srinivasan, S. *Electrochim. Acta* **1978**, *23*, 521−526.
(8) Reier, T.; Oezaslan, M.; Strasser, P. *ACS Catal.* **2012**, *2*, 1765−1772.
(9) Song, S.; Zhang, H.; Ma, X.; Shao, Z.; Baker, R. T.; Yi, B. *Int. J. Hydrogen Energy* **2008**, *33*, 4955−4961.
(10) Antolini, E.; Gonzalez, E. R. *Solid State Ionics* **2009**, *180*, 746−763.
(11) Kötz, R.; Stucki, S. *Electrochim. Acta* **1986**, *31*, 1311−1316.
(12) Roller, J. M.; Arellano-Jimenez, M. J.; Jain, R.; Yu, H. R.; Carter, C. B.; Maric, R. *J. Electrochem. Soc.* **2013**, *160*, F716−F730.
(13) Owe, L. E.; Tsypkin, M.; Wallwork, K. S.; Haverkamp, R. G.; Svein Sunde, S. *Electrochim. Acta* **2012**, *70*, 158−164.
(14) Angelinetta, C.; Trasatti, S.; Atanasoska, Lj. D.; Minevski, Z. S.; Atanasoski, R. T. *Mater. Chem. Phys.* **1989**, *22*, 231−247.
(15) Marshall, A. T.; Haverkamp, R. G. *Electrochim. Acta* **2010**, *55*, 1978−1984.
(16) Cheng, J.; Zhang, H.; Chen, G.; Zhang, Y. *Electrochim. Acta* **2009**, *54*, 6250−6256.
(17) Mayousse, E.; Maillard, F.; Fouda-Onana, F.; Sicardy, O.; N. Guillet, N. *Int. J. Hydrogen Energy* **2011**, *36*, 10474−10481.
(18) Angelinetta, C.; Trasatti, S.; Atanososka, Lj. D.; Atanasoski, R. T. *J. Electroanal. Chem.* **1986**, *214*, 535−546.
(19) Mamaca, N.; Mayousse, E.; Arrii-Clacens, S.; Napporn, T. W.; Servat, K.; Guillet, N.; Kokoh, K. B. *Appl. Catal., B* **2012**, *111*−*112*, 376−380.
(20) Li, G.; Yu, H.; Song, W.; Wang, X.; Li, Y.; Shao, Z.; Yi, B. *Int. J. Hydrogen Energy* **2012**, *37*, 16786−16794.
(21) Mattos-Costa, F. I.; de Lima-Neto, P.; Machado, S. A. S.; Avaca, L. A. *Electrochim. Acta* **1998**, *44*, 1515−1523.
(22) Felix, C.; Maiyalagan, T.; Pasupathi, S.; Bladergroen, B.; Linkov, V. *Int. J. Electrochem. Sci.* **2012**, *7*, 12064−12077.
(23) Kameyama, K.; Tsukada, K.; Yahikozawa, K.; Takasu, Y. *J. Electrochem. Soc.* **1994**, *141*, 643−647.
(24) Hutchings, R.; Müller, K.; Kötz, R.; Stucki, S. *J. Mater. Sci.* **1984**, *19*, 3987−3994.
(25) Marshall, A. T.; Sunde, S.; Tsypkin, M.; Tunold, R. *Int. J. Hydrogen Energy* **2007**, *32*, 2320−2324.
(26) Corona-Guinto, J. L.; Cardeño-García, L.; Martínez-Casillas, D. C.; Sandoval-Pineda, J. M.; Tamayo-Meza, P.; Silva-Casarin, R.; González-Huerta, R. G. *Int. J. Hydrogen Energy* **2013**, *38*, 12667−12673.
(27) Cheng, J.; Zhang, H.; Ma, H.; Zhong, H.; Zou, Y. *Int. J. Hydrogen Energy* **2009**, *34*, 6609−6613.
(28) Antolini, E. *Appl. Catal., B* **2009**, *88*, 1−24.
(29) Jang, I.; Hwang, I.; Tak, Y. *Electrochim. Acta* **2013**, *90*, 148−156.
(30) De Pauli, C. P.; Trasatti, S. *J. Electroanal. Chem.* **2002**, *538*−*539*, 145−151.
(31) Marshall, A. T.; Borrensen, B.; Hagen, G.; Tsypkin, M.; Tunold, R. *Electrochim. Acta* **2006**, *51*, 3161−3167.
(32) Xu, J.; Liu, G.; Li, J.; Wang, X. *Electrochim. Acta* **2012**, *59*, 105−112.
(33) Li, G.; Yu, H.; Wang, X.; Sun, S.; Li, Y.; Shao, Z.; Yi, B. *Phys. Chem. Chem. Phys.* **2013**, *15*, 2858−2866.
(34) Rubel, M.; Haasch, R.; Mrozek, P.; Wieckowski, A.; De Pauli, C.; Trasatti, S. *Vacuum* **1994**, *45*, 423−427.
(35) Marshall, A.; Børresen, B.; Hagen, G.; Tsypkin, M.; Tunold, R. *Mater. Chem. Phys.* **2005**, *94*, 226−232.
(36) Ribeiro, J.; Alves, P. D. P.; de Andrade, A. R. *J. Mater.Sci.* **2007**, *42*, 9293−9299.
(37) Murakami, Y.; Ohkawauchi, H.; Ito, M.; Yahikozawa, K.; Takasu, Y. *Electrochim. Acta* **1994**, *39*, 2551−2554.
(38) De Pauli, C. P.; Trasatti, S. *J. Electroanal. Chem.* **1995**, *396*, 161−168.
(39) Balko, E. N.; Nguyen, P. H. *J. Appl. Electrochem.* **1991**, *21*, 678−682.
(40) Ardizzone, S.; Trasatti, S. *Adv. Colloid Interface Sci.* **1996**, *64*, 173−251.
(41) Ardizzone, S.; Bianchi, C. L.; Cappelletti, G.; Ionita, M.; Minguzzi, A.; Rondinini, S.; Vertova, A. *J. Electroanal. Chem.* **2006**, *589*, 160−166.
(42) Kadakia, K.; Datta, M. K.; Velikokhatnyi, O. I.; Jampani, P.; Park, S. K.; Saha, P.; Poston, J. A.; Manivannan, A.; Kumta, P. N. *Int. J. Hydrogen Energy* **2012**, *37*, 3001−3013.
(43) Chen, X.; Chen, G.; Yue, P. L. *J. Phys. Chem. B* **2001**, *105*, 4623−4628.
(44) Comninellis, Ch.; Vercesi, P. *J. Appl. Electrochem.* **1991**, *21*, 136−142.
(45) Xu, L. K.; Scantlebury, J. D. *J. Electrochem. Soc.* **2003**, *150*, B254−B261.
(46) Terezo, A. J.; Pereira, E. C. *Electrochim. Acta* **2000**, *45*, 4351−4358.
(47) Kadakia, K.; Datta, M. K.; Jampani, P. H.; Park, S. K.; Kumta, P. N. *J. Power Sources* **2013**, *222*, 313−317.
(48) Datta, M. K.; Kadakia, K.; Velikokhatnyi, O. I.; Jampani, P. H.; Chung, S. J.; Poston, J. A.; Manivannan, A.; Kumta, P. N. *J. Mater. Chem. A* **2013**, *1*, 4026−4037.
(49) Lee, W. H.; Kim, H. *Catal. Comm.* **2011**, *12*, 408−411.
(50) Zhao, C.; Yu, H.; Li, Y.; Li, X.; Ding, L.; Fan, L. *J. Electroanal. Chem.* **2013**, *688*, 269−274.
(51) Ortel, E.; Reier, T.; Strasser, P.; Kraehnert, R. *Chem. Mater.* **2011**, *23*, 3201−3209.
(52) Li, G.; Yu, H.; Song, W.; Dou, M.; Li, Y.; Shao, Z.; Yi, B. *ChemSusChem* **2012**, *5*, 858−861.
(53) Zhao, C.; E, Y.; Fan, L. *Microchim. Acta* **2012**, *178*, 107−114.
(54) Hoare, I. P. *J. Electroanal. Chem.* **1968**, *18*, 251−259.
(55) Appleby, A. J. *J. Electroanal. Chem.* **1970**, *27*, 325−334.
(56) Sepa, D. B.; Vojnovic, M. V.; Stojanovic, M.; Damjanovic, A. *J. Electroanal. Chem.* **1987**, *218*, 265−272.
(57) Huang, S. Y.; Ganesan, P.; Jung, H. Y.; Popov, B. N. *J. Power Sources* **2012**, *198*, 23−29.
(58) Yang, D.; Li, B.; Zhang, H.; Ma, J. *Int. J. Hydrogen Energy* **2012**, *37*, 2447−2454.
(59) Yoshinaga, N.; Sugimoto, W.; Takasu, Y. *Electrochim. Acta* **2008**, *54*, 566−573.
(60) Chang, C. H.; Yuen, T. S.; Nagao, Y.; Yugami, H. *J. Power Sources* **2010**, *195*, 5938−5941.
(61) Yuan, W.; Tang, Y.; Pan, M.; Li, Z.; Tang, B. *Renew. Energy* **2010**, *35*, 656−666.
(62) Lee, K.; Zhang, L.; Zhang, J. *J. Power Sources* **2007**, *170*, 291−296.
(63) Qiao, J.; Li, B.; Yang, D.; Ma, J. *Appl. Catal., B* **2009**, *91*, 198−203.
(64) Zheng, J.; Wang, X.; Qiao, J.; Yang, D.; Li, B.; Li, P.; Iv, H.; Ma, J. *Electrochem. Commun.* **2010**, *12*, 27−31.
(65) Qiao, J.; Lin, R.; Li, B.; Ma, J.; Liu, J. *Electrochim. Acta* **2010**, *55*, 8490−8497.

(66) Li, B.; Qiao, J.; Yang, D.; Lv, H.; Ma, J. *ECS Trans.* **2009**, *25*, 613−618.
(67) Guo, Q.; Li, L. R.; Lu, L.; Ji, Y.; Lu, T. H. *Chem. J. Chin. Univ.* **2012**, *33*, 1007−1010.
(68) Lee, K.; Zhang, L.; Zhang, J. *Int. J. Green Energy* **2011**, *8*, 295−305.
(69) Lee, K.; Zhang, L.; Zhang, J. *J. Power Sources* **2007**, *165*, 108−113.
(70) Liu, G.; Zhang, H. *J. Phys. Chem. C* **2008**, *112*, 2058−2065.
(71) Neergat, M.; Gunasekar, V.; Singh, R. K. *J. Electrochem. Soc.* **2011**, *158*, B1060−B1066.
(72) Xu, T.; Zhang, H.; Zhang, Y.; Zhong, H.; Jin, H.; Tang, Y. *J. Power Sources* **2011**, *196*, 5849−5852.
(73) Ma, J.; Ai, D.; Xie, X.; Guo, J. *Particuology* **2011**, *9*, 155−160.
(74) Bouwkamp-Wijnoltz, A. L.; Visscher, W.; van Veen, J. A. R. *Electrochim. Acta* **1994**, *39*, 1641−1645.
(75) Bouwkamp-Wijnoltz, A. L.; Palys, B. J.; Visscher, W.; van Veen, J. A. R. *J. Electroanal. Chem.* **1996**, *406*, 195−202.
(76) Han, S. J.; Jung, H. J.; Shim, J. H.; Kim, H. C.; Sung, S. J.; Yoo, B.; Lee, D. H.; Lee, C.; Lee, Y. *J. Electroanal. Chem.* **2011**, *655*, 39−44.
(77) You, D. J.; Jin, S.; Lee, K. H.; Pak, C.; Choi, K. H.; Chang, H. *Catal. Today* **2012**, *185*, 138−142.
(78) Dembinska, B.; Kiliszek, M.; Elzanowska, H.; Pisarek, M.; Kulesza, P. J. *J. Power Sources* **2013**, *243*, 225−232.
(79) Liu, J. H.; Jeon, M. K.; Woo, S. I. *Appl. Surf. Sci.* **2006**, *252*, 2580−2587.
(80) Topalov, G.; Ganske, G.; Lefterova, E.; Schnakenberg, U.; Slavcheva, E. *Int. J. Hydrogen Energy* **2011**, *36*, 15437−15445.
(81) Ioroi, T.; Yasuda, K. *J. Electrochem. Soc.* **2005**, *152*, A1917−A1924.
(82) Holt-Hindle, P.; Yi, Q.; Wu, G.; Koczkur, K.; Chen, A. *J. Electrochem. Soc.* **2008**, *155*, K5−K9.
(83) Liu, G. C.; Sanderson, R. J.; Vernstrom, G.; Stevens, D. A.; Atanasoski, R. T.; Debe, M. K.; Dahn, J. R. *J. Electrochem. Soc.* **2010**, *157*, B207−B214.
(84) Radev, I.; Topalov, G.; Lefterova, E.; Ganske, G.; Schnakenberg, U.; Tsotridis, G.; Slavcheva, E. *Int. J. Hydrogen Energy* **2012**, *37*, 7730−7735.
(85) Huang, S. Y.; Ganesan, P.; Jung, H. Y.; Popov, B. N. *J. Power Sources* **2012**, *198*, 23−29.
(86) Toda, T.; Igarashi, H.; Uchida, H.; Watanabe, M. *J. Electrochem. Soc.* **1999**, *146*, 3750−3756.
(87) Mukerjee, S.; Srinivasan, S.; Soriaga, M. P.; McBreen, J. *J. Electrochem. Soc.* **1995**, *142*, 1409−1422.
(88) Loukrakpam, R.; Wanjala, B. N.; Yin, J.; Fang, B.; Luo, J.; Shao, M.; Protsailo, L.; Kawamura, T.; Chen, Y.; Petkov, V.; Zhong, C.-J. *ACS Catal.* **2011**, *1*, 562−572.
(89) Loukrakpam, R.; Shan, S.; Petkov, V.; Yang, L.; Luo, J.; Zhong, C.-J. *J. Phys. Chem. C* **2013**, *117*, 20715−20721.
(90) Adzic, R. R.; Zhang, J.; Sasaki, K.; Vukmirovic, M. B.; Shao, M.; Wang, J. X.; Nilekar, A. U.; Mavrikakis, M.; Valerio, J. A.; Uribe, F. *Top. Catal.* **2007**, *46*, 249−262.
(91) Brankovic, S. R.; Wang, J. X.; Adzic, R. R. *Surf. Sci.* **2001**, *474*, L173−L179.
(92) Zhang, J.; Vukmirovic, M. B.; Xu, Y.; Mavrikakis, M.; Adzic, R. R. *Angew. Chem., Int. Ed.* **2005**, *44*, 2131−2135.
(93) Gong, K.; Chen, W. F.; Sasaki, K.; Su, D.; Vukmirovic, M. B.; Zhou, W.; Izzo, E. L.; Perez-Acosta, C.; Hirunsit, P.; Balbuena, P. B.; Adzic, R. R. *J. Electroanal. Chem.* **2010**, *649*, 232−237.
(94) Karan, H. I.; Sasaki, K.; Kuttiyiel, K.; Farberow, C. A.; Mavrikakis, M.; Adzic, R. R. *ACS Catal.* **2012**, *2*, 817−824.
(95) Hirunsit, P.; Balbuena, P. B. *J. Phys. Chem. C* **2010**, *114*, 13055−13060.
(96) Knupp, S. L.; Vukmirovic, M. B.; Haldar, P.; Herron, J. A.; Mavrikakis, M.; Adzic, R. R. *Electrocatal.* **2010**, *1*, 213−223.
(97) Sasaki, K.; Kuttiyiel, K. A.; Su, D.; Adzic, R. R. *Electrocatalysis* **2011**, *2*, 134−140.
(98) Kuttiyiel, K. A.; Sasaki, K.; Choi, Y.; Su, D.; Liu, P.; Adzic, R. R. *Energy Environ. Sci.* **2012**, *5*, 5297−5304.
(99) Gu, Z.; Balbuena, P. B. *J. Phys. Chem. A* **2006**, *110*, 9783−9787.
(100) Liu, J. H.; Jeon, M. K.; Woo, S. I. *Appl. Surf. Sci.* **2006**, *252*, 2580−2587.
(101) Ma, Y.; Balbuena, P. B. *J. Electrochem. Soc.* **2010**, *157*, B959−B963.
(102) Sethuraman, V. A.; Weidner, J. W.; Haug, A. T.; Pemberton, M.; Protsailo, L. V. *Electrochim. Acta* **2009**, *54*, 5571−5582.
(103) Ma, Y.; Balbuena, P. B.; Ball, S. C.; O'Malley, R.; Theobald, B. R. C.; Izzo, E. L.; Murthi, V. S.; Protsailo, L. V. *J. Phys. Chem. C* **2013**, *117*, 23224−23234.
(104) Wesselmark, M.; Wickman, B.; Lagergren, C.; Lindbergh, G. *Electrochim. Acta* **2013**, *111*, 152−159.
(105) Oh, J.-G-; Lee, W. H.; Kim, H. *Int. J. Hydrogen Energy* **2012**, *37*, 2455−2461.
(106) Pettersson, J.; Ramsey, B.; Harrison, D. *J. Power Sources* **2006**, *157*, 28−34.
(107) Chen, G.; Delafuente, D. A.; Sarangapani, S.; Mallouk, T. E. *Catal. Today* **2001**, *67*, 341−355.
(108) Yim, S. D.; Lee, W. Y.; Yoon, Y. G.; Sohn, Y. J.; Park, G. G.; Yang, T. H.; Kim, C. S. *Electrochim. Acta* **2004**, *50*, 713−718.
(109) Zhang, Y.; Wang, C.; Wan, N.; Mao, Z. *Int. J. Hydrogen Energy* **2007**, *32*, 400−404.
(110) Rivas, S.; Arriaga, L. G.; Morales, L.; Fernandez, A. M. *Int. J. Electrochem. Sci.* **2012**, *7*, 3601−3609.
(111) Swette, L. L.; LaConti, A. B.; McCatty, S. A. *J. Power Sources* **1994**, *47*, 343−351.
(112) Shao, Z.; Yi, B.; Han, M. *J. Power Sources* **1999**, *79*, 82−85.
(113) Ioroi, T.; Kitazawa, N.; Yasuda, K.; Yamamoto, Y.; Takenaka, H. *J. Electrochem. Soc.* **2000**, *147*, 2018−2022.
(114) Ioroi, T.; Kitazawa, N.; Yasuda, K.; Yamamoto, Y.; Takenaka, H. *J. Appl. Electrochem.* **2001**, *31*, 1179−1183.
(115) Yao, W.; Yang, J.; Wang, J.; Nuli, Y. *Electrochem. Commun.* **2007**, *9*, 1029−1034.
(116) Zhang, Y.; Zhang, H.; Ma, Y.; Cheng, J.; Zhong, H.; Song, S.; Ma, H. *J. Power Sources* **2010**, *195*, 142−145.
(117) Escalante-Garcia, I. L.; Duron-Torres, S. M.; Cruz, J. C.; Arriaga-Hurtado, L. G. *J. New Mater. Electrochem. Syst.* **2010**, *13*, 227−233.
(118) Altmann, S.; Kaz, T.; Friedrich, K. A. *Electrochim. Acta* **2011**, *56*, 4287−4293.
(119) Cruz, J. C.; Baglio, V.; Siracusano, S.; Ornelas, R.; Arriaga, L. G.; Antonucci, V.; Aricò, A. S. *Int. J. Hydrogen Energy* **2012**, *37*, 5508−5517.
(120) Kong, F. D.; Zhang, S.; Yin, G. P.; Zhang, N.; Wang, Z. B.; Du, C. Y. *J. Power Sources* **2012**, *210*, 321−326.
(121) Cruz, J. C.; Rivas, S.; Beltran, D.; Meas, Y.; Ornelas, R.; Osorio-Monreal, G.; Ortiz-Frade, L.; Ledesma-García, J.; Arriaga, L. G. *Int. J. Hydrogen Energy* **2012**, *37*, 13522−13528.
(122) Kong, F. D.; Zhang, S.; Yin, G. P.; Wang, Z. B.; Du, C. Y.; Chen, G. Y.; Zhang, N. *Int. J. Hydrogen Energy* **2012**, *37*, 59−67.
(123) Kong, F. D.; Zhang, S.; Yin, G. P.; Zhang, N.; Wang, Z. B.; Du, C. Y. *Electrochem. Commun.* **2012**, *14*, 63−66.
(124) Jung, H.-Y.; Park, S.; Popov, B. N. *J. Power Sources* **2009**, *191*, 357−361.
(125) Yim, S. D.; Park, G. G.; Sohn, Y. J.; Lee, W. Y.; Yoon, Y. G.; Yang, T. H.; Sukkee Um, S.; Yu, S. P.; Kim, C. S. *Int. J. Hydrogen Energy* **2005**, *30*, 1345−1350.
(126) Fall, J.; Humphreys, D.; Guo, S. M. *J. Fuel Cell Sci. Technol.* **2009**, *6*, 0310031−0310035.
(127) Wan, C. H.; Wu, C. L.; Lin, M. T.; Shin, C. *J. Nanosci. Nanotechnol.* **2010**, *10*, 4612−4618.
(128) Huang, S.-Y.; Ganesan, P.; Jung, H.-Y.; Popov, B. N. *J. Power Sources* **2012**, *198*, 23−29.
(129) Zhang, G.; Shao, Z. G.; Lu, W.; Li, G.; Liu, F.; Yi, B. *Electrochem. Commun.* **2012**, *22*, 145−148.
(130) Garcia, G.; Roca-Ayats, M.; Lillo, A.; Galante, J. L.; Peña, M. A.; Martínez-Huerta, M. V. *Catal. Today* **2013**, *210*, 67−74.